metals

MDPI

Article

Heterogenous Grain Nucleation in Al-Si Alloys: Types of Nucleant Inoculation

Ehab Samuel, Hicham Tahiri, Agnes M. Samuel and Fawzy H. Samuel *

Département des Sciences Appliquées, Université du Québec à Chicoutimi, Saguenay, QC G7H 2B1, Canada; ehabfhsamuel@gmail.com (E.S.); hicham_tahiri@yahoo.com (H.T.); agnesmsamuel@gmail.com (A.M.S.)
* Correspondence: fhsamuel@uqac.ca

Abstract: The objective of the current work is to establish, on the one hand, the conventional mechanisms of grain refining and, on the other hand, the effect of the refining-modification interaction in Sr-modified Al-Si alloys on the achieved grain refining and the modification of eutectic silicon. For this purpose, the hypereutectic alloy A390.1 (~17%Si) was used. Various grain refiners were used, namely, Al-10%Ti, Al-5%Ti-1%B, and Al-4%B. After the preparation of the liquid metal, several concentrations of these master alloys were added to the liquid bath according to the desired objective. The different melts prepared were heated at 750 °C and cast in a preheated graphite mold with a solidification rate of around 0.8 °C/s. The liquid metal was. The presence of strontium (added in the form of Al-10%Sr master alloy) and boron completely affects the microstructure of the alloy. An atom of Sr unites with 6 atoms of B to form a compound whose stoichiometric formula is of the SrB_6 type, leading to a significant reduction in the modification. A strong relationship exists between the addition of B and the recovery level of Sr. The affinity between titanium and boron is stronger than the affinity between boron and strontium. Both B and TiB_2 phase particles do not react with Si; it is only the Ti part of the Al-Ti-B master that forms $(Al, Si)_3Ti$. Regardless of the amount of Si content in the alloy, the Al-4%B master alloy achieves the best grain refining compared to Ti-containing master alloys.

Keywords: grain refining; Sr modification; undercooling; Sr-Ti interaction; Sr-B interaction

check for updates

Citation: Samuel, E.; Tahiri, H.; Samuel, A.M.; Samuel, F.H. Heterogenous Grain Nucleation in Al-Si Alloys: Types of Nucleant Inoculation. *Metals* **2024**, *14*, 271. https://doi.org/10.3390/met14030271

Academic Editor: Noé Cheung

Received: 6 February 2024
Revised: 15 February 2024
Accepted: 20 February 2024
Published: 24 February 2024

Copyright: © 2024 by the authors. Licensee MDPI, Basel, Switzerland. This article is an open access article distributed under the terms and conditions of the Creative Commons Attribution (CC BY) license (https://creativecommons.org/licenses/by/4.0/).

1. Introduction

In terms of tonnage, although aluminum, production only represents a little more than 2% of that of steel, this metal and the alloys derived from it come in second place in terms of production and use of metallic materials. Aluminum owes this place to a set of properties which, in many circumstances, make it an irreplaceable material. During their use, metals change from a liquid to a solid state [1–6]. Additionally, the solidification of any metal or alloy can be studied by thermal analysis. The latter consists of analyzing the temperature versus time (T(t)) data collected during solidification. Thermal analysis therefore makes it possible to study different phenomena and parameters that occur during the solidification process [7–10].

Turnbull and Vonnegut [11] suggested that the heterogeneous nucleation of grains on a catalyst can be enhanced by strong lattice disregistry at the nucleation interface. The findings of Bolzoni and Hari Babu [12] indicate that the physical and chemical characteristics of the nucleant surface are more important for nucleation than the lattice disregistry. Thus, the theory of nucleation based on the theoretical model of lattice registry is not supported. Maxwell and Hellawell [13] classified the effectiveness of different particles based on an evaluation of their degree of promotion of grain refining [14–18].

In aluminum alloys, Al_3Ti particles are considered to be the main source for achieving significant grain refinement for aluminum alloys with a Ti concentration that is higher than 0.15%, i.e., peritectic reaction. Moreover, the peritectic compositions, the Al_3Ti phase

particles are not stable under equilibrium conditions. Basically, there are two sources for grain refinement as per the carbide-boride and the peritectic reaction theory [19–25]. Although boride or carbide are recognized as suitable sites for heterogenous nucleation, the Al_3Ti particles have a significant influence on the grain refinement process itself. The dissolution of Al_3Ti phase particles is required to provide excess titanium to enhance grain growth and thus establish an effective heterogeneous nucleation that can be related to the initial dissolution of Al_3Ti and proper nucleant surface conditions [26–30].

Cast alloys normally consist of large concentrations of Si or Cu, which may cause certain difficulties in achieving an acceptable grain refinement level. The introduction of alloying elements would restrict the capacity of Al-Ti-B grain refinement. The master alloys employed to refine the grains are not similar in their degree of effectiveness when used in cast alloys. As an example, the level of Al-5Ti-1B master alloy is high for obtaining full refining in cast alloys, whereas, Al-4B has been proposed to produce powerful grain refining in Al-Si cast alloys [31–51]. Although other particles have been investigated [52–57], the undercooling required to initiate solidification was minimized when Al_3Ti particles were present [58–65]. The actual evidence that any one nucleant may be associated with the initiation of solidification is not extensive.

In order to arrive at a better understanding of the role of the above-mentioned parameters in terms of grain refining of high Si- and Cu-containing alloys such as the A390.1 alloy (containing about 17%Si and 4.5%Cu), the present study was undertaken to highlight the following goals:

1. Determining the effect of different master alloys (Al-10%Ti, Al-5%Ti-1%B, and Al-4%B) on the grain size and on the morphology of the α-Al phase by varying the holding times before casting (30 min, 60 min, and 90 min).
2. Studying the consequences of the addition of grain refiners (Al-10%Ti, Al-5%Ti-1%B, and Al-%B) in small quantities on grain refining using the A390.1 alloy.
3. Identifying the effect of the interaction between the Sr modifier and the grain refiner (Al-10Ti, Al-5Ti-1B, and Al-4B), the interaction between silicon and titanium, and their competition in affecting the morphology of the eutectic silicon, on the grain size, and on the shape of the α-Al dendritic phase.
4. Investigating the Si poisoning phenomenon.

2. Experimental Procedure

The nature of the alloys and the additions of the master alloys, as well as the casting method and various techniques used in this work for the characterization of the microstructure and the identification of the different phases (i.e., electron microprobe and energy dispersive X-rays), are detailed in this article.

In this research, the A390.1 (17%Si) alloy, often chosen for the manufacturing of cylinder heads for gasoline engines and in other applications where good castability and weldability are required, was selected. The experiments carried out were divided into two distinct parts. The first part concerned the addition of various master alloys (grain refiners) to explore the conventional mechanisms of grain refinement. The second part concentrated on observing the effect of the strontium-grain refiner interaction as well as its impact on the realization of grain refinement and the modification of eutectic silicon.

In order to carry out grain refining and study the effectiveness of each of the grain refiners, three master alloys in the form of small waffles were used for this purpose, namely: Al-10%Ti, Al-5%Ti-1%B, and Al-4%B. These master alloys were added so that the weight percentage of titanium (Ti) or boron (B) was 0.02, 0.04, 0.06, 0.08, and 0.1%. Melts were degassed using pure Ar that was injected using a rotating graphite impeller (130 rpm) for about 30 min. Due to the high oxidation reactivity of Sr, the element was added as an Al-10%Sr master alloy in the form of rods only 5 min prior to casting, i.e., towards the end of degassing. All A390.1 alloy melts prepared were poured after a suitable stirring time. A single casting temperature, 750 °C, was applied. Figure 1a–c shows the size and distribution of Al_3Ti, AlB_2, and TiB_2 in their respective master alloys.

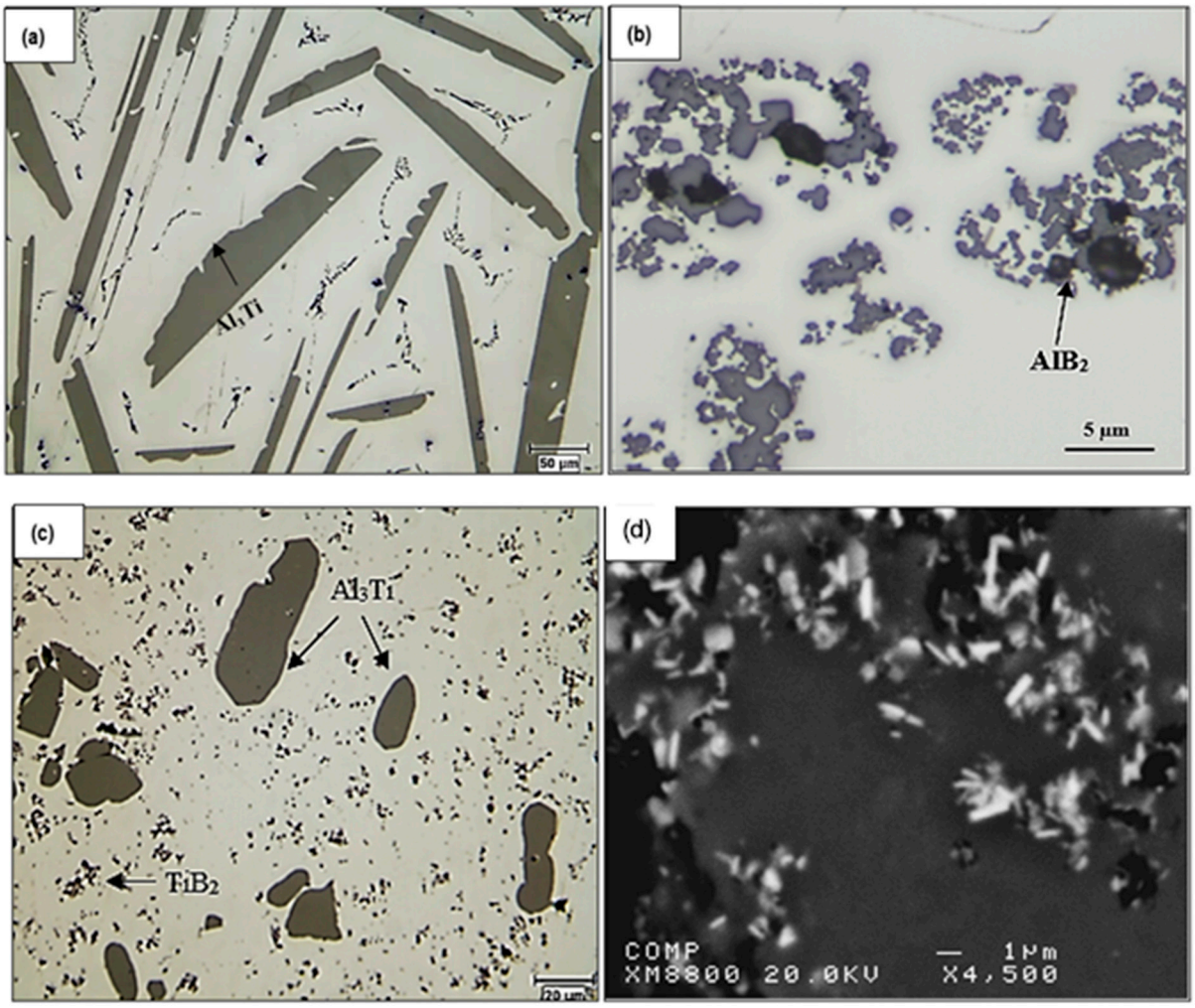

Figure 1. (**a**) Al- 10%Ti, (**b**) Al-4% B, (**c**) Al-5%Ti-1%B master alloys, (**d**) TiB_2 distribution in (**c**). Note the difference in the size of the Al_3Ti platelets in (**a**,**c**).

The data relating to the thermal analysis were measured using type K thermocouples (OMEGA Canada, St-Eustache, QC, Canada), 0.3 mm in diameter. During solidification, the data was recorded using a computer, allowing high-speed data acquisition at five measurements per second. For the Al-4%B alloy, the additions were made in a sequence ranging from 0 ppm to 1000 ppm B. The contact time between the liquid metal and the AlB_2 boron nucleation sites before casting is half an hour, following a suitable stirring period. Figure 2 shows the position of the thermocouple in the graphite mold in which all the alloys were cast. The chemical composition of the alloy is given in the following Table 1 (all elements are in % by weight).

Table 1. Chemical composition of the used A390.1 alloy (wt. %).

Alloy	Al	Si	Cu	Mg	Fe	Mn	Zn	Ti	P (ppm)
A390.1	bal.	17.30	4.33	0.54	0.32	0.06	0.06	0.07	25

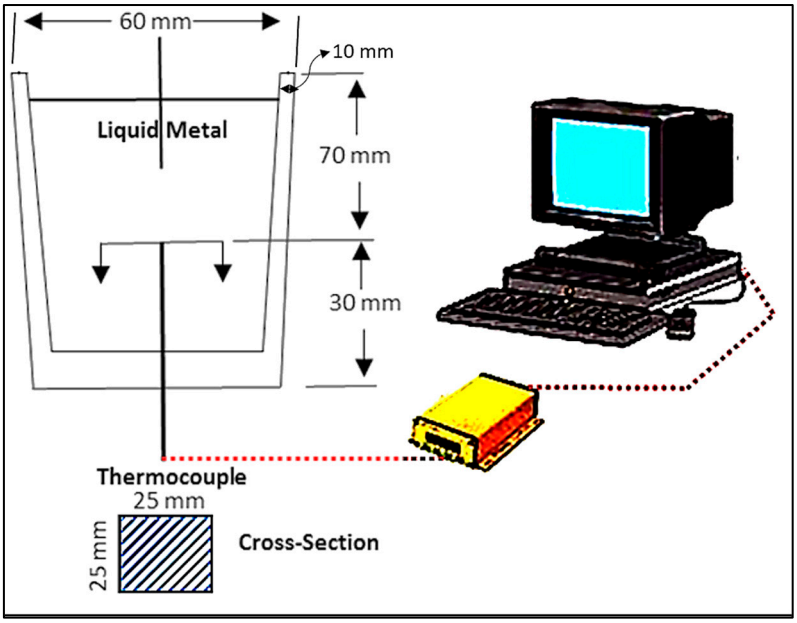

Figure 2. Schematic drawing showing the graphite mold used for thermal analysis.

To study the microstructure and the various phases that were obtained, corresponding to the different solidification conditions, samples with a dimension of 2 cm × 3 cm (as shown in Figure 2) were cut near the thermocouple tip, then pelletized and polished for metallographic examination. Using a mixture of acids with appropriate percentages (66% HNO_3, 33% HCl, and 1% HF), the surface of the samples from the A390.1 alloy series was chemically etched so that the grain size could be measured. To have a slow attack, a quantity of water was added to the mixture of acids. Once the chemical attack is complete, the specimens are photographed using a special montage. Concerning the chemical attack for the samples of the A390.1 alloy series, a mixture of 50% H_2O, 25% HNO_3, 15% HCl, and 10% HF was used.

3. Results and Discussion

3.1. Results

3.1.1. Thermal Analysis

The temperature-time solidification curve and its first derivative obtained from the hypereutectic alloy A390.1 are presented in Figure 3. Based on the phase diagram of the Al-Si binary system, during solidification, the first precipitation is related to the deposition of primary silicon particles in the form of large particles (100 to 150 µm), as illustrated in Figure 4a.

Table 2. Reactions in hypereutectic A390.1 (17%Si) (adapted from Ref. [58]).

Peak	Reactions	Temperature (°C)
A	Primary Si	670
B	Development of a dendritic network	561
C	Liq. → Al + Si + Al_5FeSi	575
D	Liq. → Al + Si + Mg_2Si	555
E	Liq. + Mg_2Si → Al + Si + Al_2Cu + $Al_5Mg_8Cu_2Si_6$	512
F	Liq. → Al + Al_2Cu +$Al_5Mg_8Cu_2Si_6$	507

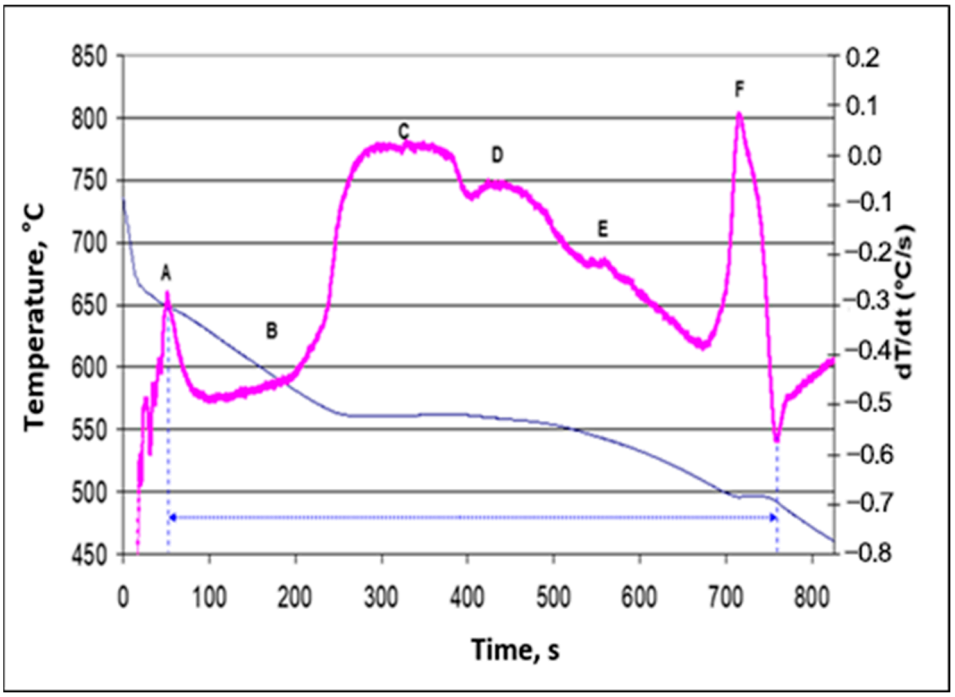

Figure 3. Temperature-time solidification curve (blue) and its first derivative (magenta). The labels A through F correspond to the reactions listed in Table 2.

As for the precipitation of the α-Al dendritic phase, it occurs over a range of temperatures, making it difficult to reveal the actual temperatures of germination and growth of this phase in a precise manner. The formation of the phases continues this time with the phase of eutectic silicon, followed by the appearance of intermetallics of magnesium and copper since this alloy contains enough Mg and Cu (4.8% by weight). The presence of titanium with a content of 2% by weight is significant enough in the base alloy to offer a certain refinement to the dendritic phase.

The detailed reactions with their suggested temperatures during solidification are given in Table 2. The eutectic zone shows the eutectic silicon, needles of the Al_5FeSi phase, a large amount of Al_2Cu, and some $Al_5Mg_8Cu_2Si_6$-type particles. The formation of the majority of Mg_2Si intermetallics appears to have been accomplished during reaction 5. Solidification is completed after the formation of the copper eutectic phase.

Hypereutectic Al-Si alloys exhibit a strongly desirable combination of characteristics, such as castability, a low coefficient of thermal expansion, corrosion resistance, and good machinability. The high concentration of silicon in these alloys is primarily responsible for many of these characteristics. However, the small size and uniform distribution of silicon particles are essential to achieving optimum alloy properties.

Primary silicon in hypereutectic alloys is not readily nucleated by the impurities that are usually present in the alloys. The reduction in size of primary silicon is normally completed by the addition of phosphorus (P) to the liquid metal. Phosphorus reacts with liquid aluminum to produce finely dispersed AlP-like compounds. The latter have a crystal structure very similar to that of silicon and react as heterogeneous nucleation sites for silicon. The addition of phosphorus is usually carried out by the introduction of Cu-P-type master alloys, where the percentage of P varies from 1 to 15% by weight. Other elements, such as Mg, W, S, and La, have been reported to be effective modifiers, but none have achieved commercial importance. Figure 4b,c show evidence for the presence of P and Ti within the phosphorus particle. Figure 4d reveals the presence of a few Ti particles acting as sites for primary Si precipitation.

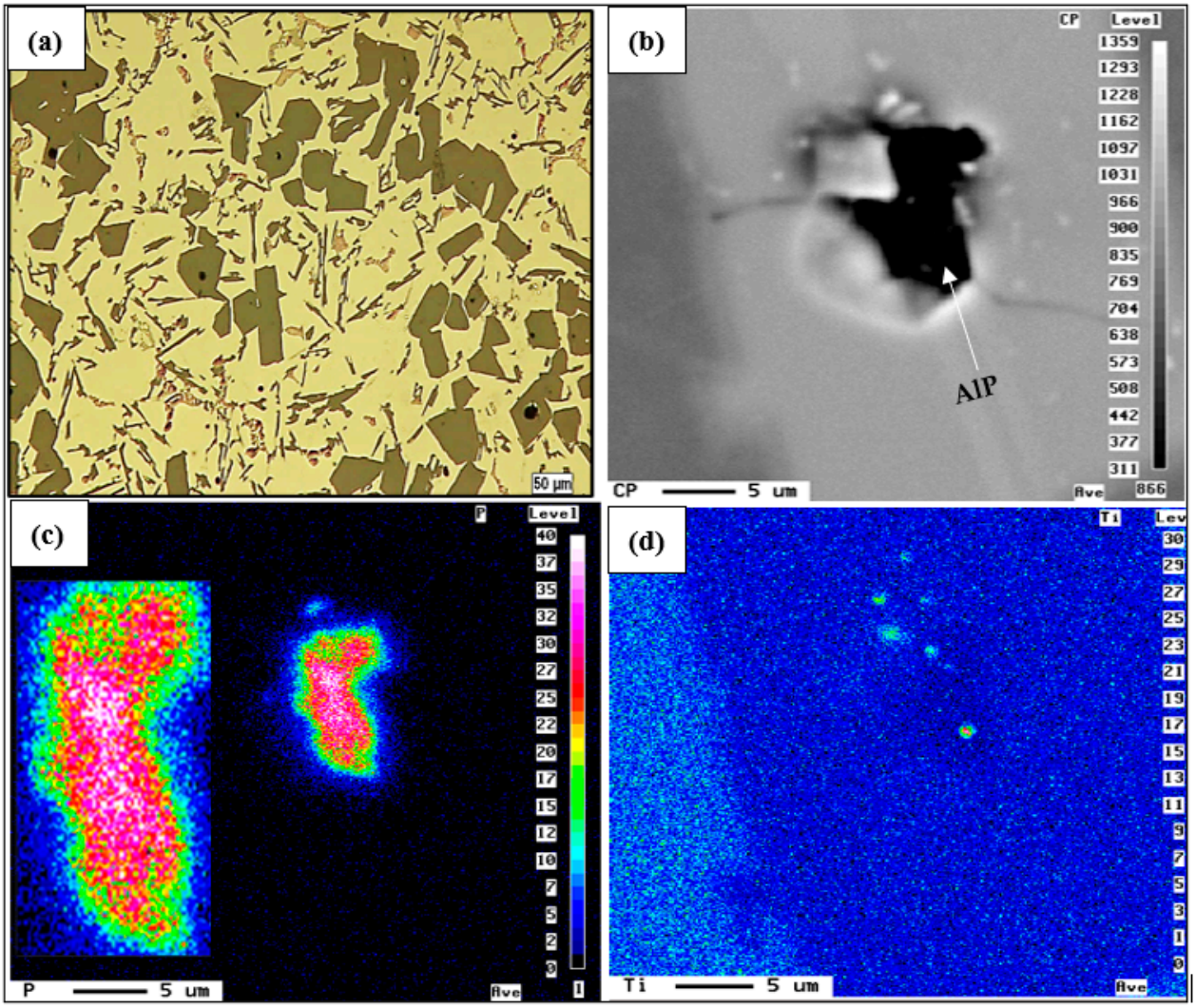

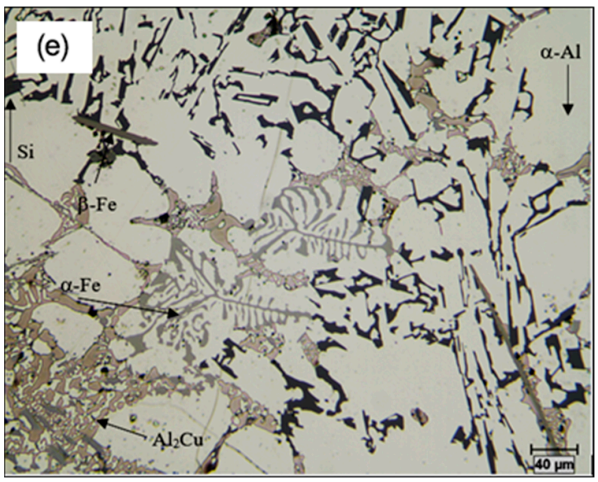

Figure 4. (**a**) Optical microstructure of solidified A390.1 alloy, (**b**) backscattered electron image of a Si particle showing a black spot identified as AlP (**c**) with Ti particles, (**d**) the inset micrograph in (**c**) depicts the presence of the Ti particles within the AlP particle, identified more clearly in the enlarged map in (**d**). (**e**) Optical micrograph describing the phase-rich microstructure of an A390 alloy treated with 0.4%Ti (Al-10%Ti).

The microstructure of hypereutectic alloy 390 mainly consists of large blocks of primary silicon, large primary grains of α-Al, including dendrites, and interdendritic networks of acicular eutectic silicon of Al_2Cu copper intermetallics formed along the interdendritic region. The unmodified acicular structure of silicon acts as an internal stress pipeline in the microstructure and provides an easy path for fracture, which is the primary reason for the low hardness level of these alloys. Figure 4e provides an overview of the microstructure of the A390 alloy treated with 0.4% Ti and cast after 30 min of holding time. As can be seen, the particles of the eutectic silicon are far from being modified, given the large percentage of silicon present in this hypereutectic alloy (~17%Si) and the insufficient quantity of strontium added for the modification. The main phases are shown by arrows. Indeed, in addition to the aluminum matrix, we find the primary silicon in the form of blocks, iron phases such as α-Fe called "Chinese writing", the eutectic silicon, the copper phase Al2Cu, the copper phase titanium in TiSi2 form, and other phases such as Mg_2Si and β-Fe (Al_5FeSi).

3.1.2. Ti-Si Interaction

It is well known that certain alloying and impurity elements in aluminum alloys can compromise the grain refinement efficiency of Al-Ti-B master alloys, particularly super-stoichiometric grain refiners such as Al-5%Ti-1%B, which contain TiB_2 and Al_3Ti particles. This deleterious effect is usually called the "poisoning effect" [66,67]. Silicon is a typical element that can poison grain refining with the addition of a titanium-rich master alloy, as mentioned by Li et al. [57] and Spittle et al. [58]. It has been observed that, during the realization of grain refinement in Al-Si casting alloys, when the silicon content exceeds 7% by weight, beginnings of grain coarsening occur, and the magnitude of the poisoning effect worsens with increasing silicon content.

To reduce this effect, an effective method is to increase the addition level of the master alloy of Al-5%Ti-1%B in order to preserve more particles of aluminides and borides unchanged by the behavior of poisoning [59,68,69]. However, increasing addition levels is a costly solution. Another approach is to reduce the titanium content in the master alloys. In fact, some new master alloys, such as Al-3%Ti-3%B, Al-1%Ti-3%B, Al-3%B, etc., provide better grain refining performance than the conventional Al-5%Ti-1%B master alloy [14,60,70–73]. A few other elements, such as magnesium, strontium, etc., have also been reported to effectively counteract the "poisoning effect" of silicon.

$TiSi_2$ phases are the major cause of such poisoning, and Figure 5 confirms the occurrence of these phases. However, since boron cannot be detected by energy-dispersive X-ray spectroscopy (EDS), the possibility of the formation of borides cannot be ignored. Applying the EDS technique, the $TiSi_2$ phase could be identified by the high intensity peaks due to Ti and Si elements. Figure 5 depicts the distribution of Ti and Si in A390.1 allloy treated with 0.4% Ti and poured after 120 min. The EDS spectrum showing the main elements in the $TiSi_2$ phase is presented in Figure 5e, whereas the corresponding data is listed in Table 3.

Table 3. Identification of the $(Al,Si)_2Ti$ phase in the hypereutectic A390.1 alloy.

Elements (at %)		
Al	**Ti**	**Si**
9.49	32.02	58.15
8.64	32.28	58.30
9.51	32.02	58.14
~8.95	~32.28	~58.30

The SrB_6 and TiB_2 phase particles could act as nucleants, but it should be noted that the consumption of boron in the compound is one of the main parameters to consider. It means that AlB_2 consumes less boron in comparison with SrB_6. Considering a constant quantity of boron, the density of the nucleating particles is much higher in the case of AlB_2,

since a lower number of boron atoms is associated with this compound. Therefore, the greater the number of effective nucleants, the greater the probability of having a smaller grain size [74].

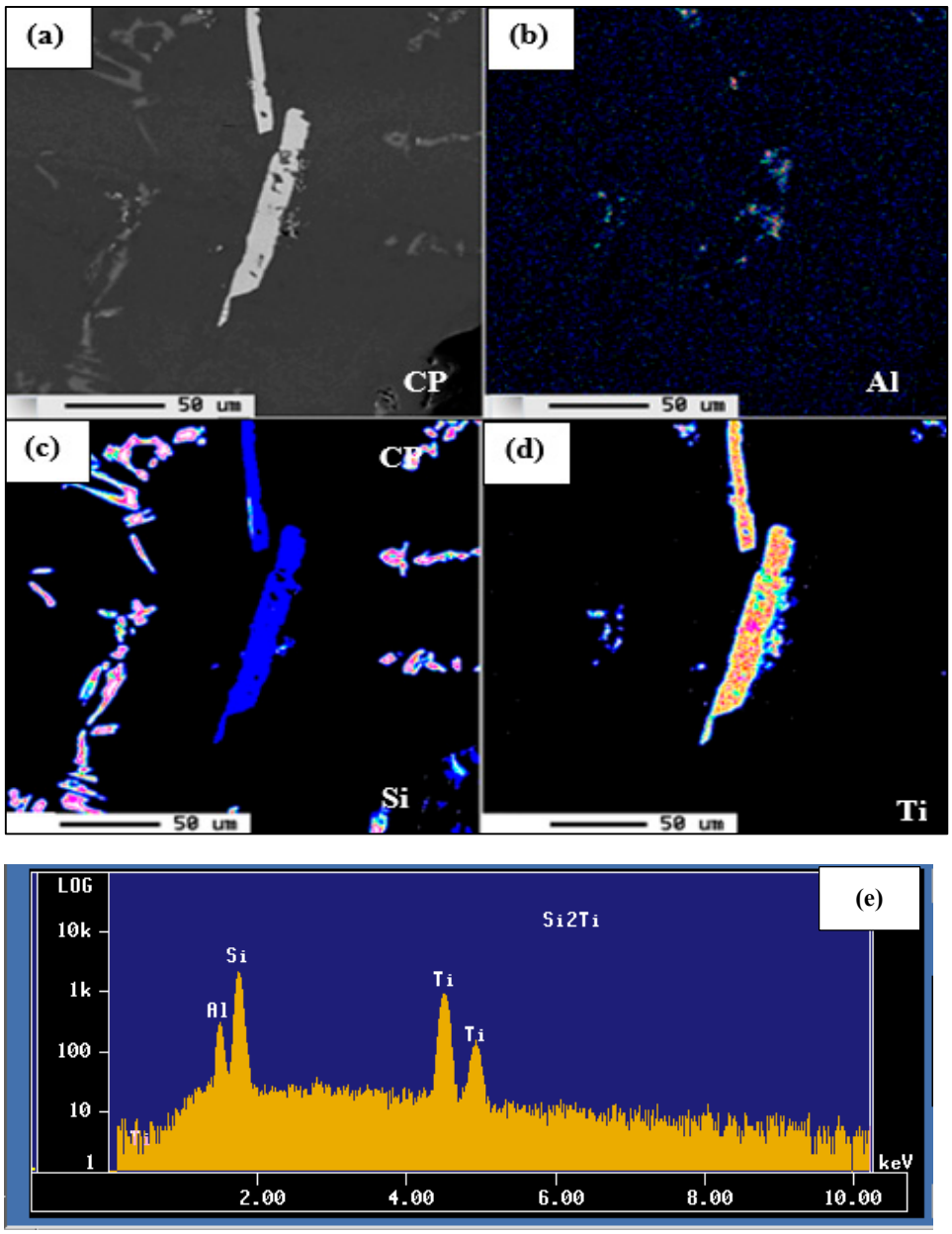

Figure 5. (**a**–**d**) Conversion of Ti platelets into $TiSi_2$ platelets without changing their morphology. (**e**) Energy dispersive X-ray (EDX) analysis of the $TiSi_2$ phase proven by the high intensity of Si and Ti peaks (Figure 4a) with a relatively smaller peak due to Al.

Using dispersion X-ray analysis, the SrB_6 phase is identified and confirmed by high intensity peaks in an A390.1 sample treated with 0.2%Ti in the form of Al-5%Ti-1%B master alloy and 200 ppm Sr. The strong affinity between strontium and boron is shown in Figures 6 and 7, obtained using the electron microprobe. The size of SrB_6 compounds varies between 5 and 10 µm, and their color is a mixture of dark gray and white. It should be borne in mind that it is not necessary that all Al_3Ti particles will convert to $Al_3(Ti,Si)$, only in high Si-containing alloys exceeding 7%. Figure 8 depicts the distribution of Ti, B, and Si in the A356 alloy, where the Si-containing particles are those of eutectic Si. On the other hand, if Sr is added in an excess amount (over modification), it is likely to precipitate

in the form of Al_2SrSi_2 particles on the pre-existing Ti particles, as shown in Figure 9. In this case, Sr was only observed on the Al-Ti boundaries, with no noticeable diffusion into the TiB_2 particles. This observation was made clear in samples treated with 0.2%Ti in the form of Al-10%Ti master alloy and 200 ppm Sr, as shown in Figure 10, which reveals no reaction between Sr and Ti. The only case when SrB_6 phase particles were abundantly clear was when the alloy was grain refined with Al-4%B master alloy (Figure 11) since B has no affinity to react with Si, in addition to the absence of Ti except for the Ti that was initially present in the received alloy. In confirmation of these observations, Figure 12 exhibits the degradation in the modification of the A356 alloy when B (Figure 12a) and Ti (Figure 12b) were added individually in the form of Al-4%B and Al-10%Ti, respectively.

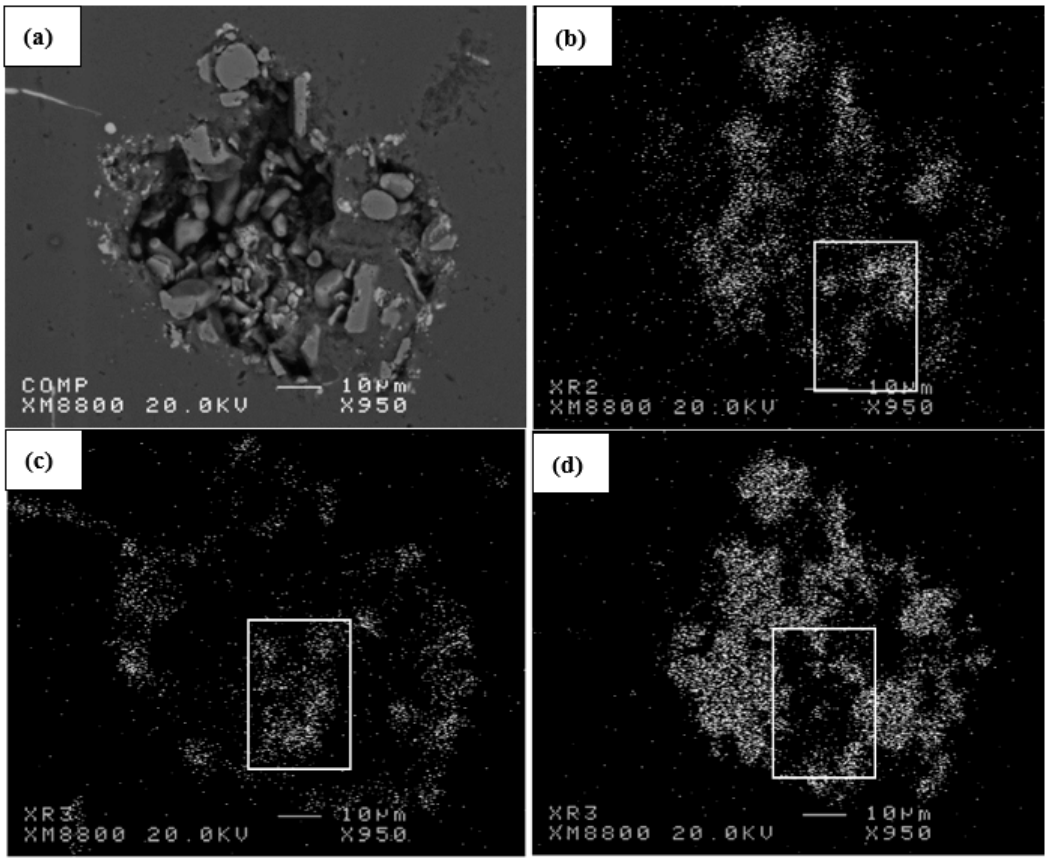

Figure 6. (**a**) Backscattered electron image of TiB_2 in grain refined-Sr modified alloy (viewed in a pore); (**b**–**d**) distribution of B, Sr, and Ti, respectively. The white square in (**b**) shows the area used to generate the Eds spectrum in Figure 7.

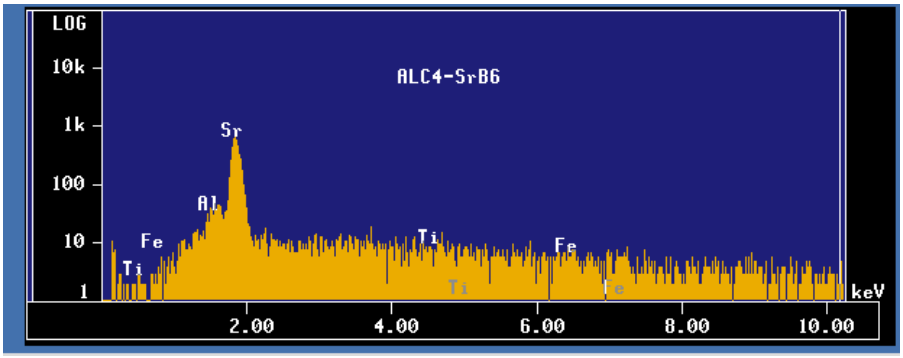

Figure 7. Dispersion X-ray (EDS) analysis of the SrB_6 phase in Figure 6a.

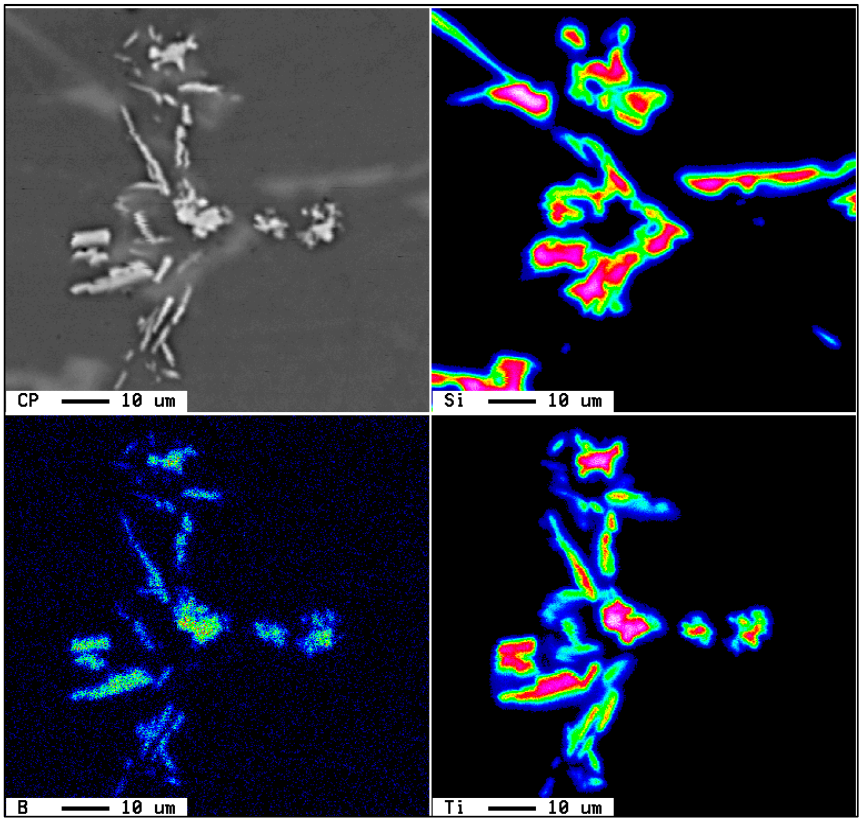

Figure 8. Distribution of Ti, B, and Si in TiB_2 particles added to the A356 alloy in the form of the Al-5%Ti-1%B master alloy. Note the absence of Si in the TiB_2 particles.

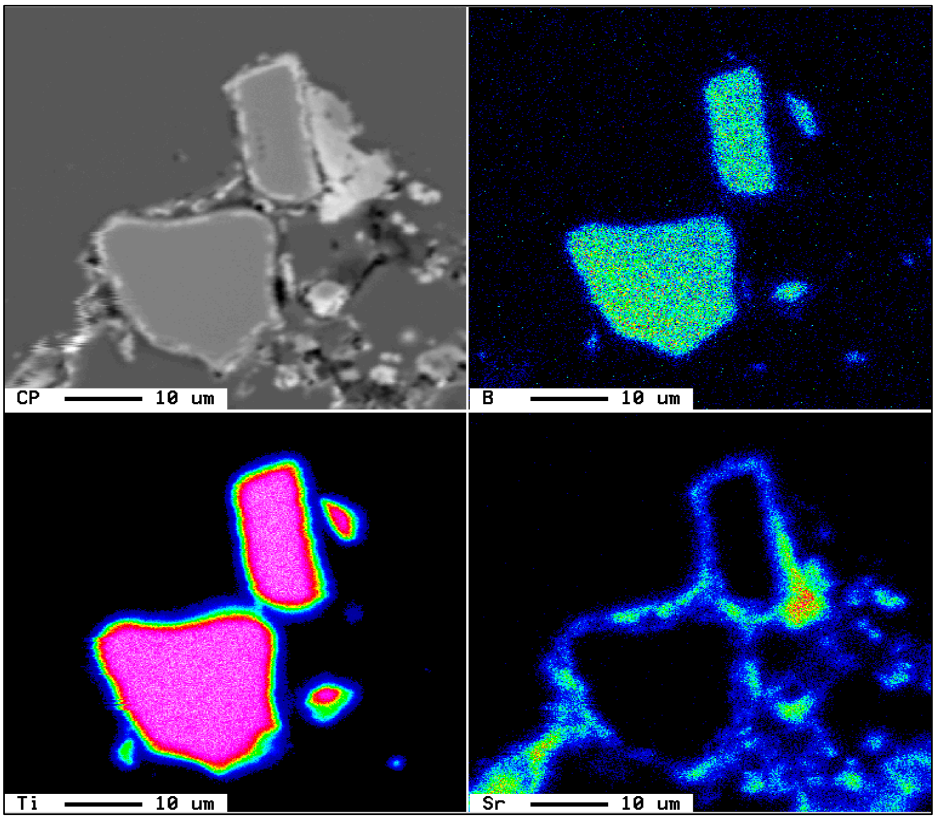

Figure 9. Precipitation of Al_2SrSi_2 particles on the edges of the pre-existing TiB_2 particles.

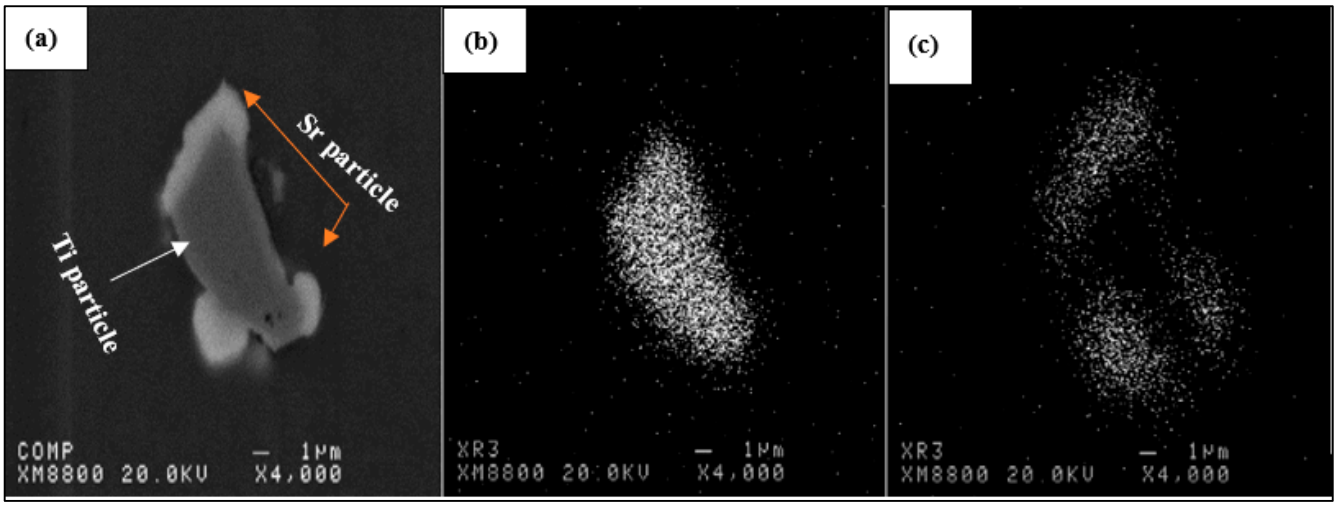

Figure 10. (**a**) Backscattered electron image of (**a**) Ti-rich particle surrounded by Sr-rich particles, (**b**,**c**) distribution of Ti and Sr in (**a**), respectively. Note the absence of Sr within the Ti image.

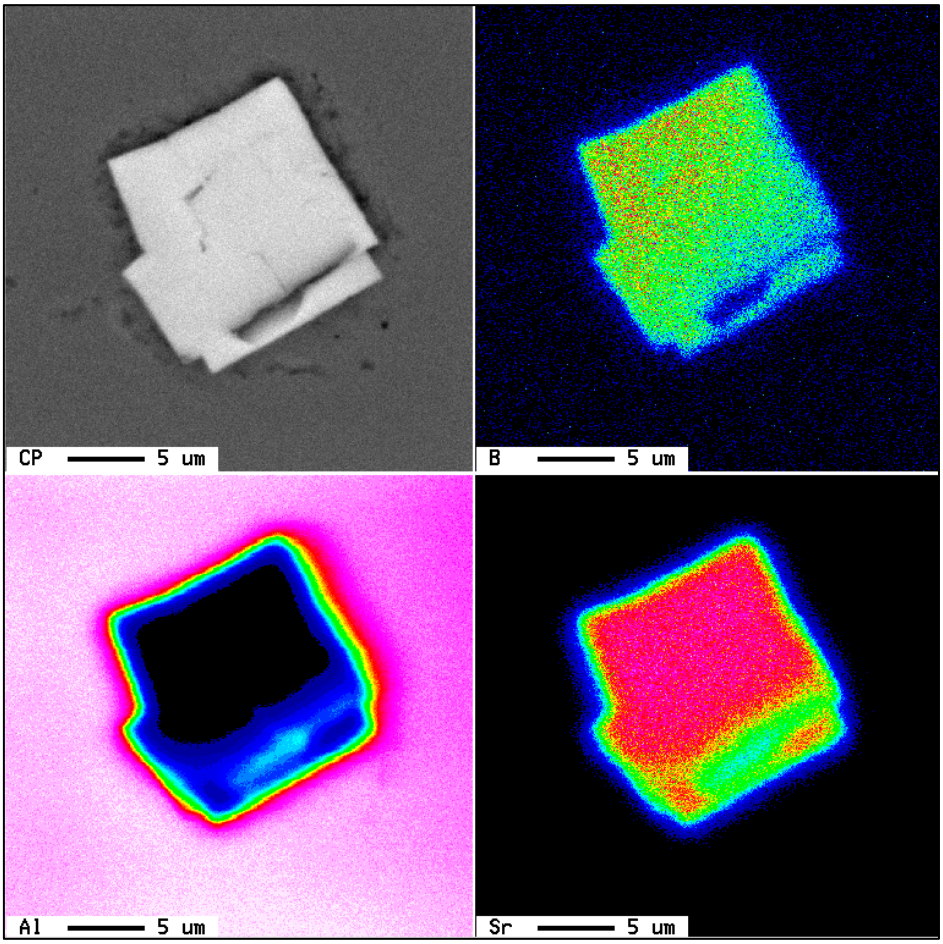

Figure 11. X-ray maps showing the Sr-B interaction forming the SrB_6-type phase in the A356 alloy.

Based on the above discussion, it is reasonable to state that after the addition of strontium and boron to the alloy (as there is a strong affinity between these two elements), they react and form SrB_6. Therefore, most of the boron atoms that should be used for refining are consumed to form this compound. The SrB_6 intermetallics have a low "disregistration coefficient" [14] with the matrix, but their boron consumption is high (six atoms), and

this is the reason why efficient refining is not fully achieved compared to that obtained in non-modified alloys. On the other hand, due to this reaction, free strontium is removed from the liquid aluminum, and therefore there is less strontium available for modification. The result obtained is indeed a partial modification.

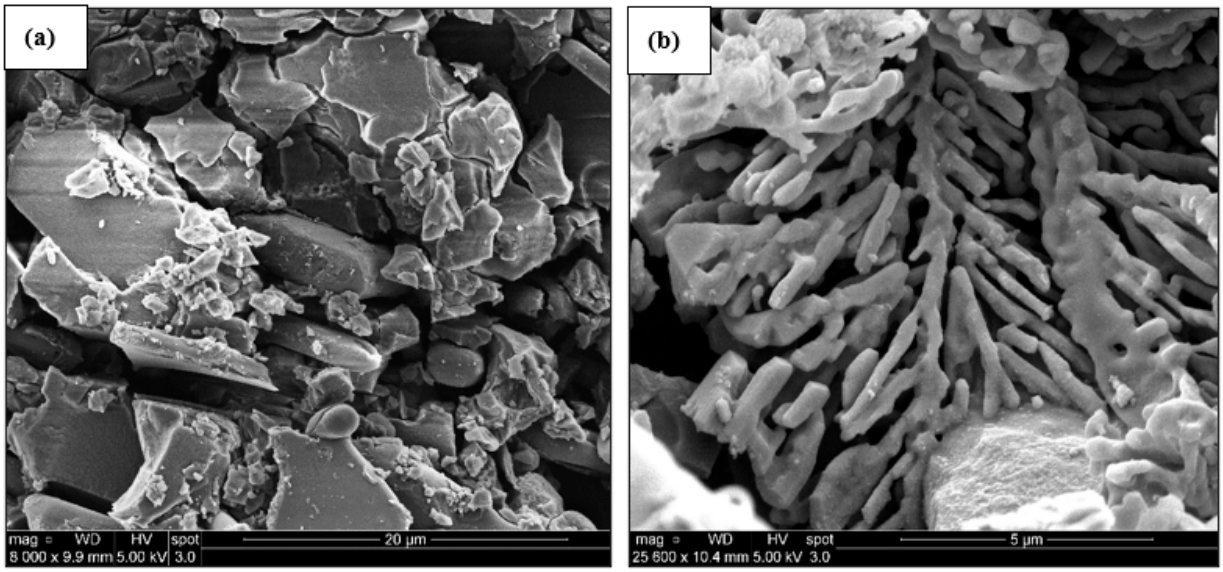

Figure 12. Optical micrographs representing the effect of liquid metal treatment on the shape of silicon in the A356 alloy: (**a**) 200 ppm Sr + 0.1%B, (**b**) 0.1% Ti, 200 ppm Sr.

3.1.3. Influence of Combined Sr and Grain Refiner Treatment on Grain Size

The microstructure of a hypereutectic alloy of type A390.1 (~17% Si) exhibits various phases and intermetallics dispersed in the aluminum matrix. In an unmodified alloy, silicon is found in two different forms: primary silicon (block form) and eutectic silicon, which takes an acicular shape as shown in Figure 13a. A complete modification is very far from being realized since the quantity of strontium added is of the order of 200 ppm while the percentage of silicon is 17% by weight. The primary silicon remains intact, given its size and quantity in the matrix. Still at the microstructure level, the dendritic phase in an unmodified alloy changes morphology from an elongated or stretched shape (see Figure 13b) to a shape of rounded rosettes in the presence of the modifier, especially in combination with a grain refiner, as shown in the circled areas in Figure 13c. A sample of untreated alloy A390.1 shows a heterogeneous distribution of the α-Al dendritic phase with randomly arranged dendrites.

After the addition of titanium and/or boron, it was observed that these elements can break down the elongated structure of the dendritic phase, causing a cell-like structure—Figure 13d.

The formation of grain size in the hypereutectic alloy A390.1 is shown in Figure 14. In the base alloy, the grains reach a value varying from 1450 to 1600 µm. The addition of 0.1% Ti in the form of Al-10%Ti to the base alloy leads to a reduction in the grain size to about 1200 µm. It is also observed that a gradual loss of reduction in grain size occurs with the successive increase in the added amount of Ti and the extension of the holding time of the liquid metal due to the formation of $(Al,Si)_2Ti$ type phases, which results in an acute decrease in grain refiner effectiveness. Specimens treated with 0.4% Ti and 200 ppm Sr and maintained for 120 min offer a maximum granular size (~1375 µm). These titanium disilicide phases deprive the Al_3Ti particles of their role in acting as nucleation sites for the α-Al dendritic phase. Figure 14 illustrates these observations.

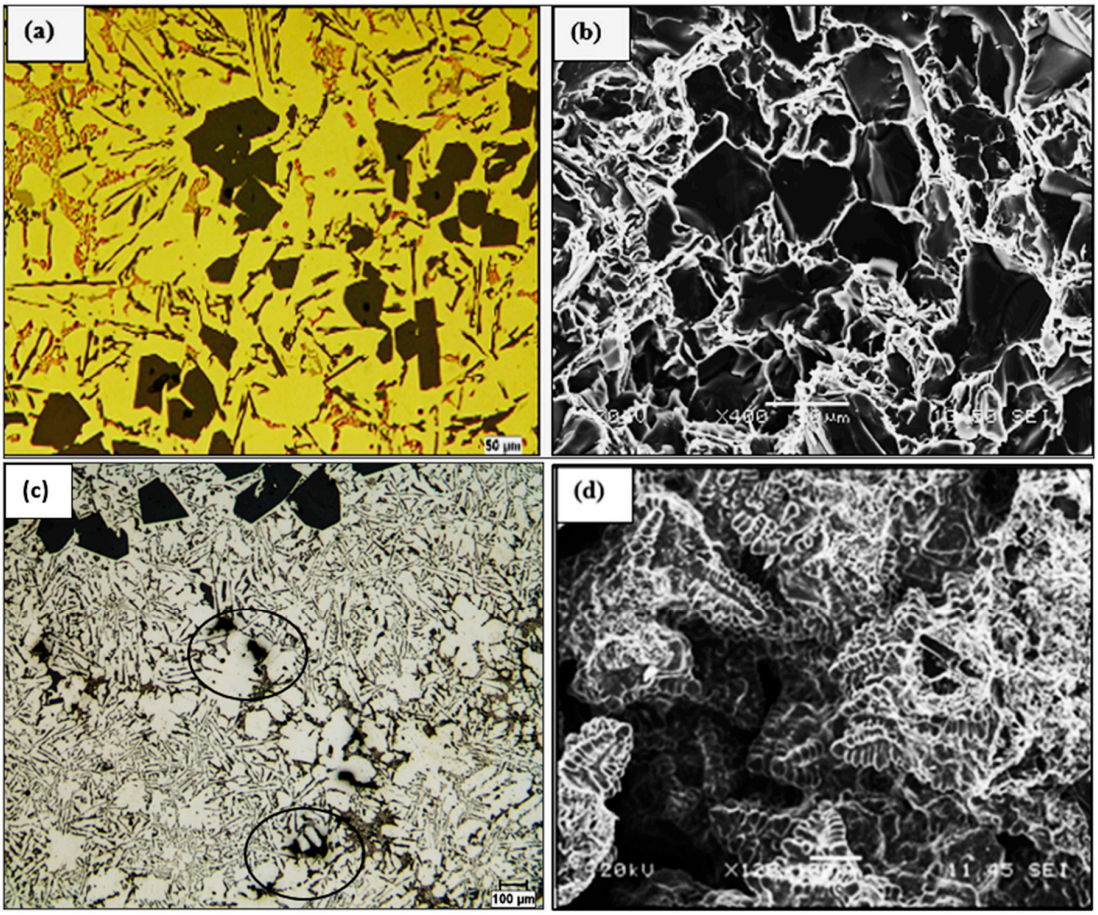

Figure 13. Microstructure of alloy A390.1: (**a**) unmodified alloy, (**b**) shape after coarsening (base alloy), (**c**) alloy treated with 200 ppm Sr, (**d**) formation of dendritic structure. Note in (**c**), eutectic Si particle shape is not fully fibrous (i.e., only partially modified).

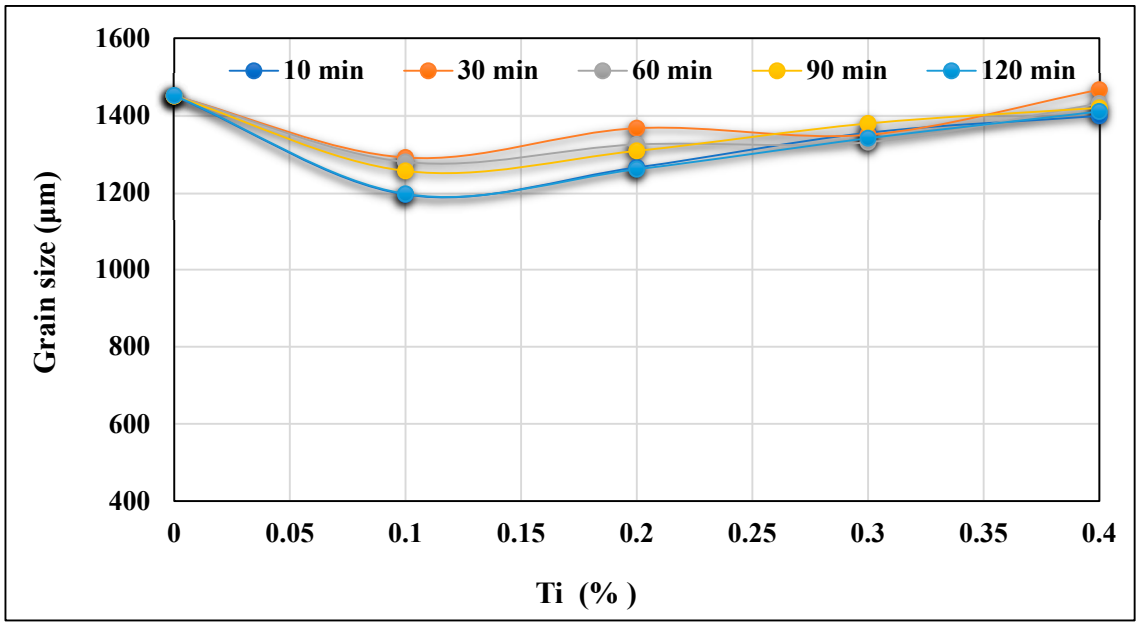

Figure 14. Variation of granular size in 390 samples treated with 200 ppm Sr and progressive additions of Ti in Al-10%Ti form.

Figure 15a represents the variation in grain size in a series of alloys A390.1 treated this time with 200 ppm Sr in addition to progressive additions of titanium and boron using the master alloy Al-5%Ti-1%B. An addition of 0.1% Ti and 0.02%B combined with 200 ppm Sr to the base alloy drops its grain size to approximately 800 µm. This represents a small reduction since the base alloy is characterized by grains whose size ranges from 1450 to 1600 µm.

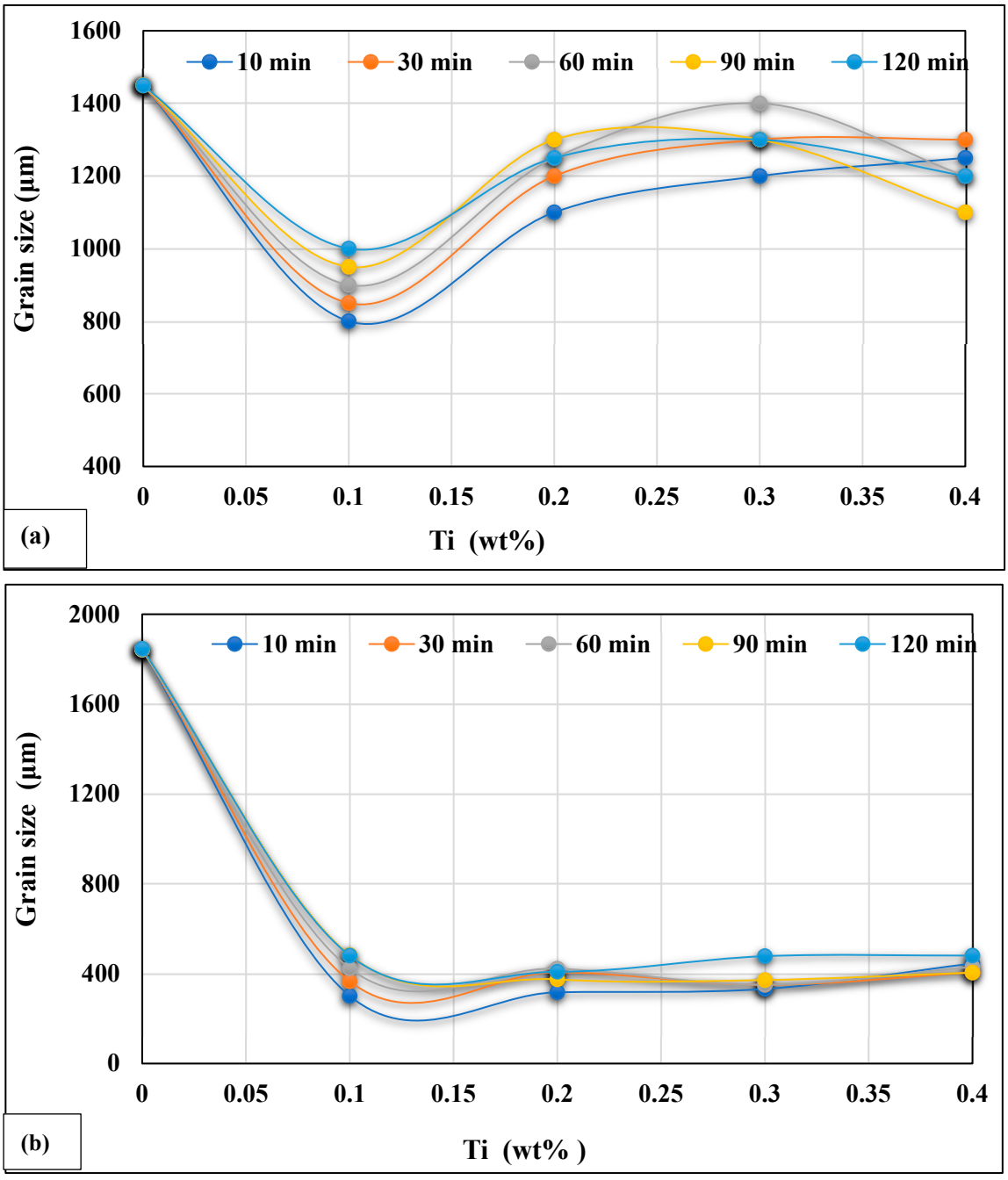

Figure 15. (**a**) Variation of grain size in samples treated with 200 ppm Sr and progressive additions of Ti and B using Al-5%Ti-1%B: (**a**) A390.1 alloy (55% maximum reduction in initial grain size), (**b**) A356.2 alloy (80% maximum reduction in initial grain size).

Maintaining the liquid metal has a negative impact on the reduction of grain size since the latter increases as a function of the increase in the liquid bath maintenance time. Even if the content of the Al-5%Ti-1%B master alloy increases, the granular size does not

undergo a big change, and it is almost constant for a given holding time. A specimen treated with 200 ppm Sr, 0.4%Ti, 0.08%B and cast after two hours of waiting shows a maximum grain size (700 µm). As the Al-5%Ti-1%B grain refiner generates two nucleation sites (Al_3Ti and TiB_2) for the pre-eutectic α-Al phase, these locations are strongly influenced by the high affinity between titanium and silicon on the one hand (formation of $TiSi_2$) and by the partial interaction existing between TiB_2 and strontium on the other hand. These interactions combine to reduce, as much as possible, the grain refining power of the master alloy, Al-5%Ti-1%B. Figure 15b depicts the same condition on grain size behavior in an A356.2 alloy containing about 7%Si and no Cu. As can be seen, in contrast to the A390.1 alloy, there is no noticeable increase in the grain size following the addition of 0.1 %Ti in the form of the Al-5%Ti-1%B master alloy.

The combined processing of the A390.1 alloy series by strontium and boron has a very remarkable influence compared to the two grain refiners mentioned before. Indeed, as described for the hypoeutectic alloy A356, boron and the modification agent react with each other to form SrB_6 type compounds. Although these two elements consume as many boron and strontium atoms, this does not prevent grain refinement from being carried out since the size of the latter decreases to a value of approximately 500 µm. This value obtained corresponds to an addition of 0.1% B by weight and a holding time of 10 min. Samples held for periods of 10 to 60 min are characterized by similar grain sizes, while samples held for extended periods before being cast adopt coarse grain sizes. Figure 16 summarizes these observations.

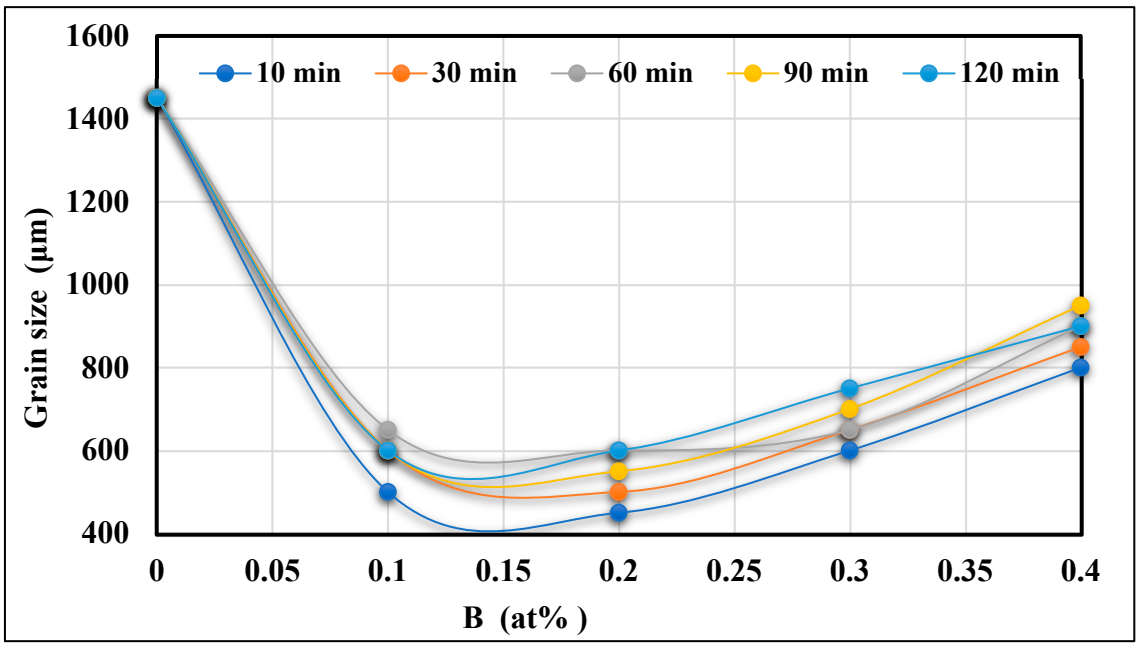

Figure 16. Evolution of grain size in specimens of hypereutectic alloy A390.1 treated with 200 ppm Sr and increasing boron additions in the form of Al-4%B master alloy.

In the absence of any treatment of the liquid metal, the grain size in pure aluminum is large and is of the order of approximately 2800 µm. When 7%Si by weight is added, this same size drops to reach a value of 1854 µm. However, in the hypereutectic alloy A390.1 (~17%Si), the grain size ranges between 1450 µm and 1600 µm. This suggests that silicon acts as a refiner in the absence of the usual grain refiners (Al-Ti-B). This result is well aligned with those obtained by Li et al. [57]. On the other hand, and in general, the grain size increases as a function of the increase in the silicon content in alloys whose grains are refined by titanium and/or boron. This leads us to believe that silicon acts as an element that poisons the effects of grain refiners. The aspects of silicon "poisoning" are very varied. We mainly note the segregation of the titanium disilicide $TiSi_2$ on the

surface of the Al_3Ti phases or by covering the {0001} surfaces of the TiB_2 particles. Silicon also decreases the solid-liquid (S-L) interfacial energy, which decreases the contact angle during heterogeneous nucleation. Moreover, silicon is known for its very low value in terms of grain growth restriction, or grain restriction factor (GRF) of about 5.9, compared to titanium, which is characterized by a high GRF (245.5).

An overview of the shape of the grains in the hypereutectic alloy A390.1 is given in Figure 17. When the binary alloy Al-10%Ti is introduced into a hypoeutectic alloy (7%Si), the Al_3Ti intermetallics from the grain refiner dissolve the silicon, and their formula becomes $(Al,Si)_3Ti$. When this same master alloy (Al-10%Ti) is introduced into a hypereutectic alloy (17%Si), this last phase is converted into a new phase of the type $(Al,Si)_2Ti$. Figure 18 represents the variation in the composition of the Al_3Ti phase (change in the atomic percentage of aluminum and silicon in the Al_3Ti phase) as a function of the weight percentage of silicon in the alloy. We clearly notice that the atomic percentage of aluminum is falling to be replaced by titanium and mainly by silicon. Figure 19 summarizes these variations.



Figure 17. Macrostructures of A390.1 alloy following (**a**–**d**) different melt additions—as noted below each macrograph.

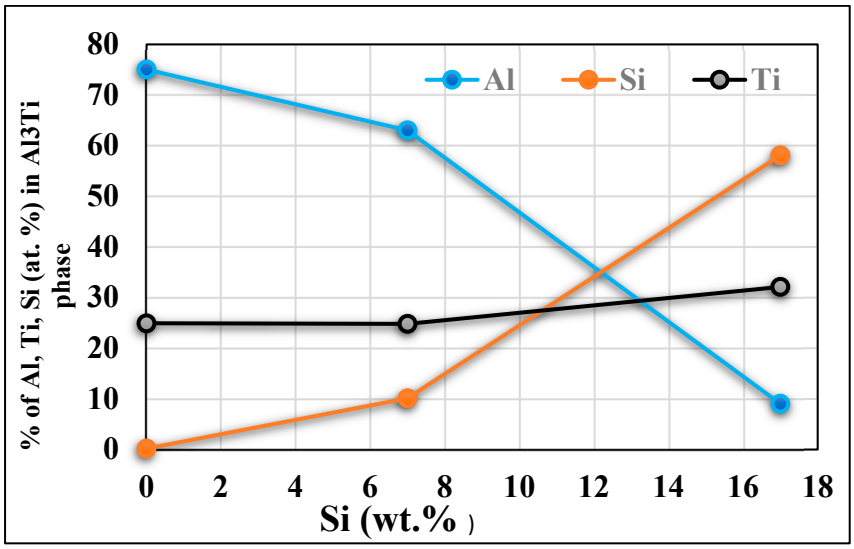

Figure 18. Variation of the composition of the Al_3Ti phase depending on the silicon content.

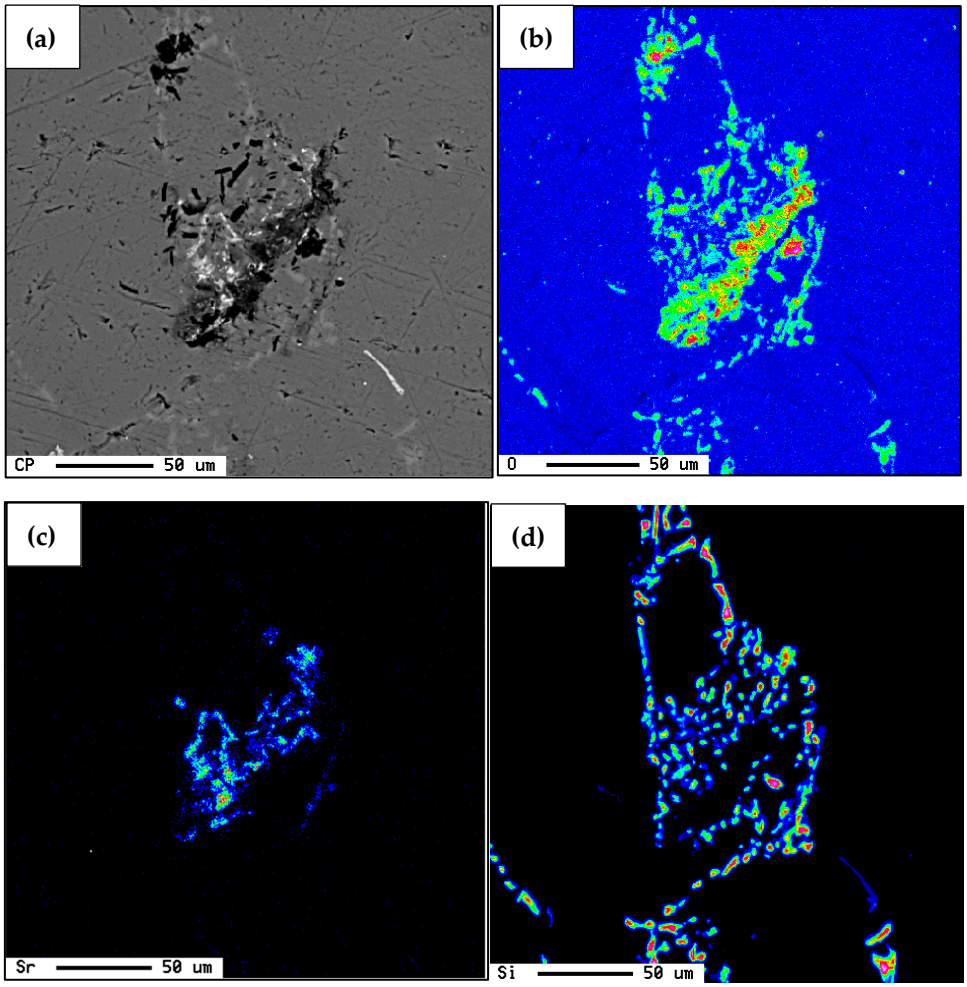

Figure 19. Entrapment of Sr with Al_2O_3 oxide films: (**a**) backscattered electron image, (**b**–**d**) distribution of O and Sr, and Si, respectively.

However, according to Qiu et al. [67], while it is rather difficult to find and identify the poisoning compound by directly employing the scanning electron microscope or transmission electron microscope, it is relatively easy to study the effect of poisoning with systematic crystallographic research into possible intermetallic compounds. According to their approach, the addition of an Al-Ti-B type master alloy to Al-Si alloys containing more than 2 wt% Si can lead to the formation of five intermetallic compounds containing silicon, i.e., Ti_5Si_3, $TiSi_2$(C49), $TiSi_2$(C54), $Al_{12}Si_3Ti_5$, and $Al_5Si_{12}Ti_7$. Crystallographic research using a very precise model indicates that only Ti_5Si_3 shows relatively weak crystallographic matching with the aluminum matrix. Therefore, Ti_5Si_3, rather than the other four silicides, is suggested as the compound most likely to cause the poisoning effect in Al-Si casting alloys. Being a compound that decreases the degree of grain refinement, Ti_5Si_3 poisons more Al_3Ti nucleation substrates than TiB_2 because, from a crystallographic point of view, the dihedral matching between Ti_5Si_3 and Al_3Ti is reasonably good, while that between $Ti5Si_3$ and TiB_2 is far from ideal.

On the other hand, as strontium is a more active oxidizing agent than aluminum, a significant part of the oxides formed during casting will generate Sr-oxides. It turns out that the Sr-oxides do not contribute to the modification of the eutectic silicon phase, although strontium is still present quantitatively in the liquid bath. Thus, once the strontium oxide is formed, a good part of the eutectic silicon remains unmodified. Additionally, the presence of Sr oxides will result in high levels of strontium recovery.

Figure 19 shows the association of strontium and oxygen in one area, and the dispersion of silicon in another area. As a result, the silicon does not undergo a major modification since the strontium is spread far from the silicon-forming oxides of the Al_2SrO_3 type. These oxides are the product of the strong affinity that exists between strontium and oxygen. The stoichiometric formula of these oxides was identified by wavelength dispersion spectroscopy.

4. Discussion

4.1. Silicon Poisoning Phenomenon

The effect of dissolved elements on the growth of the solid can be measured by the parameter Q:

$$Q = \Sigma m_i C_0,i(k_i - 1)$$

where m_i, c_0, i, and k_i represent the slope of the liquidus, the initial concentration of each element (assumed to be i elements in total), and the partition coefficient, respectively.

A higher value of the latter exposes inoculant particles to very large undercooling, and therefore a higher fraction of particles becomes active, favoring a fine and equiaxed microstructure. The effect of solute grain refinement is attributed to constitutional undercooling, which slows dendrite growth due to diffusion of the solute to the front of the interface until activation of other locations where nucleation takes place. However, increasing levels of silicon can cause coarse grain structure (silicon poisoning) in aluminum alloys refined with Al-Ti-B master alloys, as mentioned by Sigworth and Guzowski [59]. The "poisoning" effect of silicon in Al-Si alloys has numerous aspects. Various mechanisms are suggested for silicon "poisoning. Among the most important aspects of this phenomenon are rate enhancement, ternary aluminide, surface tension, and silicide (segregation) mechanisms.

Figure 20 depicts the variation in the density of eutectic Si particles as a function of the type and amount of added grain refiner as well as the stirring time for the Sr-modified A390.1 alloy. It is evident from this figure that addition of the Al-B or Al-Ti-B master alloy leads to the consumption of a significant amount of Sr, causing partial modification, as indicated by the drop in the density of Si particles from 2300 particle/mm^2 to only 400 particles/mm^2, whereas the addition of 0.4%Ti added in the form of Al-10%Ti master alloy reduced it to about 1300 particles/mm^2 due to poor Ti-Sr interaction. Apparently, stirring time has no significant effect in playing any role on this process, as demonstrated in Figure 21 [71–74].

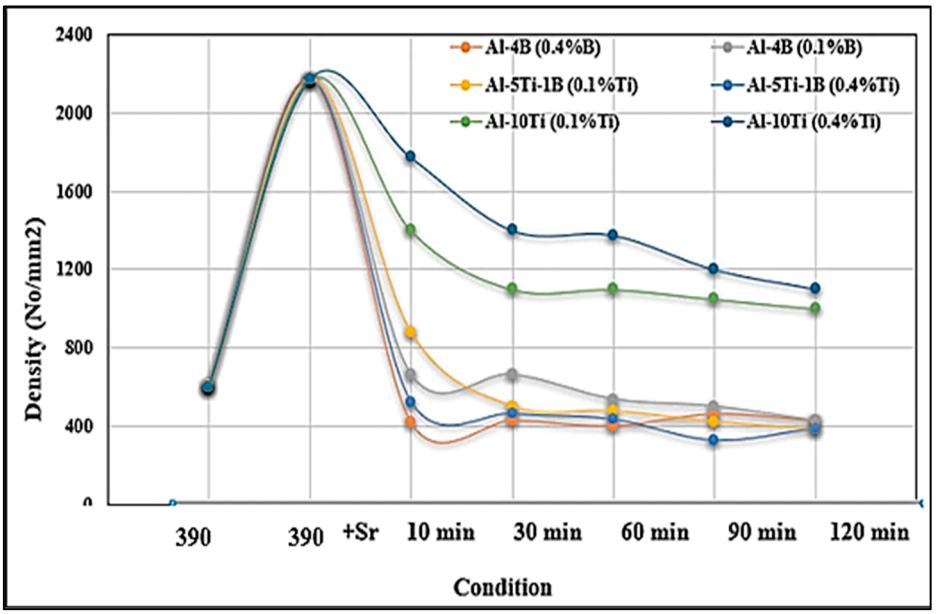

Figure 20. Variation of density of eutectic Si particles as a function of type and amount of added master alloy.

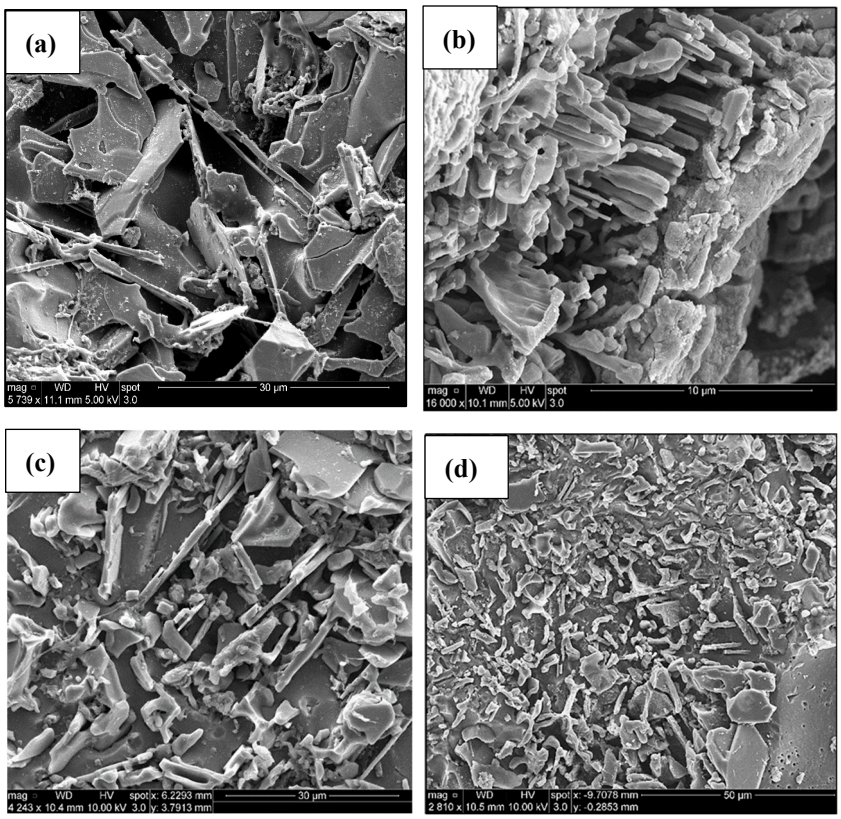

Figure 21. A390.1 alloy treated with 260 ppm Sr and grain refined with B or Ti: (**a**) non-modified alloy, (**b**) Sr-modified alloy, (**c**) grain refined with 0.4%B in the form of Al-4%B master alloy, and (**d**) grain refined with 0.4% Ti in the form of Al-10%Ti master alloy. The stirring time was about 20 min.

4.2. Mechanism for Improving Dendrite Growth Rate

Johnsson [75] suggested that higher levels of silicon cause an increase in dendrite growth rate. The increase in grain size occurs at a similar level of silicon, thus causing changes in morphology (from globular to dendrite). It has been proposed that the sharper end of a dendrite can disperse the solute more efficiently and thus grow more quickly. It is well known that when a small number of solutes that are well partitioned are added to pure liquid metal, dendrite velocities can be increased. The origin of this effect can be understood in terms of the stability criterion. According to this criterion, freezing turns out to be linked to speed Y by:

$$Y = \left(\Delta SD/2\pi^2 Q\gamma\right)\cdot\Delta {T_s}^2$$

and,

$$Q = m\cdot c_0\cdot(k-1)$$

where ΔS is the entropy of fusion per unit volume, γ is the solid-liquid interface energy, ΔTs is the undercooling, and Ds is the diameter of the solidified crystal. Since the radius of marginal stability is significantly larger than the critical core radius, curvature freezing can be reasonably neglected. It is evident that the growth rate under the stated conditions is inversely proportional to the growth restriction parameter [75].

The addition of the dissolved body to pure liquid aluminum increases the morphological instability of the dendritic tip, and according to the marginal stability analysis, this tip can grow with a smaller radius. With very low dissolved substance contents, the growth of the solid is limited by the diffusion of heat rather than by the diffusion of the dissolved substance. In this regime, when the diffusion of solutes itself does not significantly prevent the growth of the solid, the sharper tip of the dendrites caused by the addition of solutes allows the latent heat to spread rapidly further, allowing faster growth.

The conditions for this speed enhancement have been intensively analyzed by Sumalatha et al. [73,74], which prove that as the solute is added to a pure liquid metal, the dendrite velocity at a given bulk freezing temperature first increases and subsequently decreases. As the solute content is increased, solute diffusion becomes the limiting factor in crystal growth, and the normal solute growth restriction effect is evident. It can be concluded that speed refinement is not suitable for conventional grain refinement of alloys. It is only found for a very low total content of dissolved substances (~50 ppm), in which grain refinement would not be possible.

Despite this conclusion, rate refinement has often been called upon to explain variations in grain refinement. Johnsson et al. [76] proved that the growth-restricting effect of the solute appears to correspond inversely to high values of total Q. These authors] have also shown an increase in grain size for alloys with 3 wt% silicon. Therefore, it is very likely that this granular increase is associated with silicon. Greer et al. [24,26] concluded that this increase in grain size is related to a specific effect of silicon in poisoning the nucleation stage of grain refinement. They mentioned that the speed enhancement effects are only known to give maximum speed as the solute content is increased, and the effects can be seen only when the solute quantity is very low.

Moreover, the globular to dendritic transition in other binary aluminum systems is not accompanied by an increase in grain size and opposes the growth behavior. Furthermore, Johnsson et al. [76] did some thermal analysis experiments to measure dendritic growth rates supporting this mechanism, but they did not explain the temperature variations across the sample, resulting in the solidification that occurs towards the edge of the sample.

4.3. Ternary Aluminide Mechanism

Another mechanism is proposed to explain the silicon "poisoning" mechanism. Indeed, silicon, in addition to titanium, could segregate on the surface of the inoculant. This results in ternary aluminides of the form $Ti(Al_{1-x},Si_x)_3$ forming on the boride. It was also suggested that high levels of silicon (more than 7%) resulted in a shift in the temperature

of the peritectic reaction to such a low temperature that the used Al-5%Ti-1%B master alloy had no power to refine the α-Al dendritic phase. The conversion of Al_3Ti platelets to $(Al,Si)_3Ti$ ones can take place either by the addition of Ti to the molten metal in the form of Al-10%Ti or Al-5%Ti-1%B master alloys or by injecting Al3Ti powder into the molten bath.

On the other hand, the addition of Al_3Ti-type powder leads to the formation of wafers containing silicon whose stoichiometric formula is $(Al,Si)_3Ti$. The latter are characterized by a formation temperature of around 740 °C. As this temperature is high, these platelets are expected to be thick and have a coarse size since the diffusion of atoms in the liquid bath is easy at this temperature and the elements can arrange and unite in large quantities almost without obstacles to form such platelets. In an A356 alloy injected with powdered Al_3Ti particles, a map carried out by the electron microprobe (Figure 22) proves the existence of silicon in situ in aluminum and titanium [60].

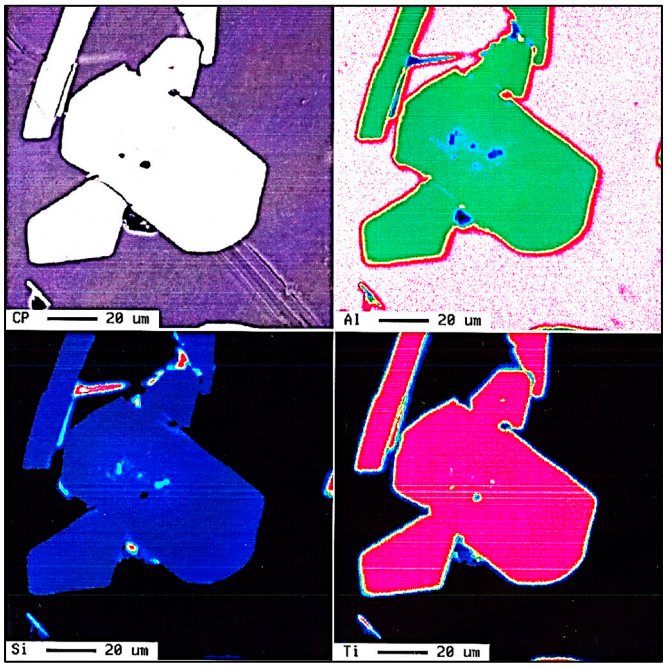

Figure 22. Mapping of an A356 sample injected with Al_3Ti powder exhibiting the distribution of Al, Si, and Ti in the new phase particles.

4.4. Surface Tension Mechanism

The energetics of heterogeneous nucleation can be described by different interfaces and the modified cluster volume involved in nucleus formation. In terms of the cluster formation shown in Figure 23, the free energy change during heterogeneous nucleation is expressed by:

$$\Delta G(r)_{het} = V_{SC}\Delta G_V + A_{SL}\sigma_{SL} + A_{nS}\sigma_{nS} - A_{nL}\sigma_{nL}$$

where V_{SC} is the spherical cap volume and A_{SL}, A_{nS}, and A_{nL} are the solid-liquid, nucleant-solid, and nucleant-liquid interfacial areas, respectively.

Sumalatha et al. [73] reported that this "poisoning" effect created by silicon leads to a reduction of the solid-liquid interfacial energy in the presence of silicon, consequently decreasing the contact angle (θ) during heterogeneous nucleation. They proved that grain size increases with contact time, contradictory to this mechanism and to the rate enhancement mechanism, because these two mechanisms are expected to be time-invariant. The nucleation of α-Al by the Al-Ti-B grain refiner cannot be analyzed using the classical heterogeneous model, as mentioned by prior investigators.

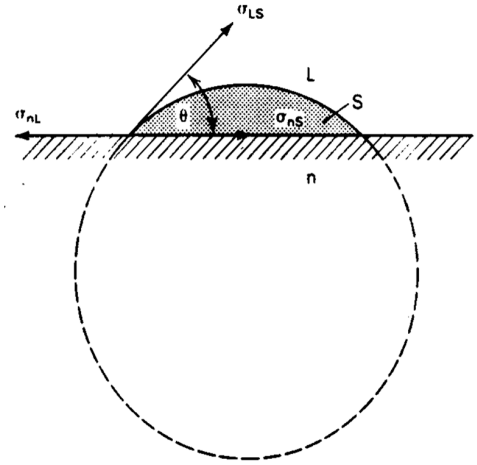

Figure 23. Relationships between a planar nucleant substrate (n), a spherical solid (S), and the liquid (L).

4.5. Mechanism of Silicide Segregation

Sigworth and Guzowski [59] suggested that titanium silicide segregates on the surface of $TiAl_3$ and poisons the efficiency of the nuclei present in the applied Al-Ti type alloy. Schumacher and McKay [60] suggested that the titanium disilicide $TiSi_2$ covers the {0001} faces of the TiB_2 particles in the liquid metal containing master alloys of the Al-5%Ti-1%B type. This silicide "poisoning" would make the TiB_2 particles incapable of nucleating the α-Al dendritic phase. Their experimental evidence for this mechanism was obtained from an observation of the rapid quenching of an aluminum alloy containing TiB_2 particles with excessive titanium. Their results showed that a good orientation ratio exists between silicide and boride. The authors also attributed the formation of the silicide phase to excessive Ti [77]. Their proposed mechanism for silicon "poisoning" appears to be reasonable. Due to the high density of Ti compared to that of Al, the precipitation of Al_3Ti platelets to the bottom of the crucible is frequently observed, as shown in Figure 24 in alloys grain refined with Al-10% Ti master alloy.

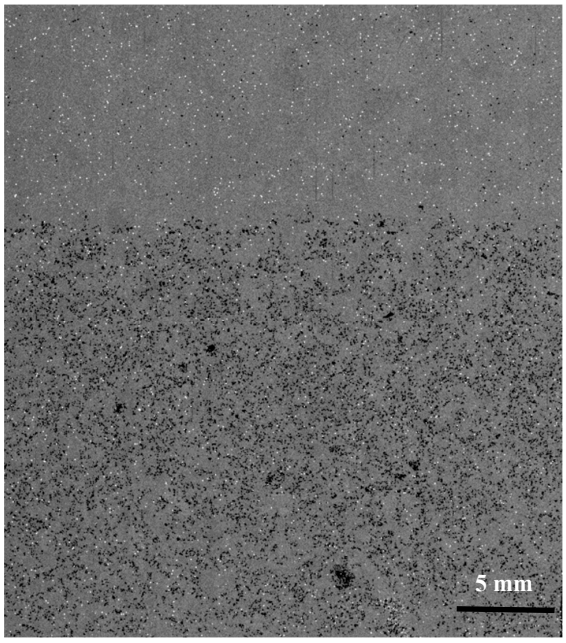

Figure 24. Sedimentation of Al_3Ti particles in a solidified casing of A390.1 alloy after holding for 5 h at 680 °C.

Other approaches to understanding grain refinement and Si poisoning include the works of Li et al. [78] in Al-10%Si alloys using 0.1 wt.%Nb Al-5Nb-B as the inoculating refiner, and that of Bian et al. [77] on Al-Si alloys using electron beam melting.

5. Conclusions

Based on the present findings, the following conclusions could be drawn:

- The same addition of Ti in the hypereutectic alloy A390.1, cast after 10 min, reduces its initial grain size (varying from 1450 to 1600 µm) to approximately 1150 µm, equivalent to a percentage reduction of almost 20% to 30%. This reduction is followed by a slight increase depending on the progressive additions of Ti and the time the liquid bath is maintained.
- Titinum addition to hypereutectic alloys results in the conversion of a good percentage of Al_3Ti intermetallics into an $(Al,Si)_2Ti$ type form containing only 9 at% Al.
- The new phase $(Al,Si)_2Ti$ influences the degree of nucleation of the dendritic phase and therefore decreases the degree of grain refinement. This phase of titanium and aluminum disilicide tends to form more when the liquid metal is maintained for long periods since its surface fraction increases remarkably as a function of the holding time of the liquid bath.
- The affinity between titanium and boron is stronger than the affinity between boron and strontium. All borides (AlB_2, SrB_6, and TiB_2) have been found to be strong grain refiners leading to about an 80% reduction in the size of the original grains.
- The formation of SrB_6 results in the degradation of the Si-modification process.

Author Contributions: Conceptualization, F.H.S. and A.M.S.; methodology, H.T. and E.S.; formal analysis, H.T. and E.S.; investigation, E.S., H.T. and A.M.S.; data curation, H.T. and E.S.; writing—original draft and preparation, F.H.S. and A.M.S.; writing—review and editing, A.M.S.; supervision, F.H.S.; project administration, F.H.S.; funding acquisition, F.H.S. All authors have read and agreed to the published version of the manuscript.

Funding: This research received no external funding.

Data Availability Statement: Data will be made available upon request.

Acknowledgments: The authors would like to thank Amal Samuel for enhancing the quality of the figures used in the present work.

Conflicts of Interest: The authors declare no conflict of interest.

References

1. Majumder, A.; Chatterjee, D.; Nandy, S. On the primary silicon precipitation during the eutectic solidification of Al-Si alloys. *Model. Simul. Mater. Sci. Eng.* **2023**, *31*, 075004. [CrossRef]
2. Peng, Q.; Zhang, Y.; Wenner, S.; Yang, B.; Milkereit, B.; Broer, J.; Springer, A.; Schick, C.; Keßler, O. Rapid solidification of Al-Si alloys using differential fast scanning calorimetry. *J. Alloys Compd.* **2023**, *965*, 171346. [CrossRef]
3. Noga, P.; Skrzekut, T.; Wędrychowicz, M. Microstructure and Mechanical Properties of Al-Si Alloys Produced by Rapid Solidification and Hot Extrusion. *Materials* **2023**, *16*, 5223. [CrossRef] [PubMed]
4. Paulin, I.; Donik, C.; Cvahte, P.; Godec, M. Bimodal Microstructure Obtained by Rapid Solidification to Improve the Mechanical and Corrosion Properties of Aluminum Alloys at Elevated Temperature. *Metals* **2021**, *11*, 230. [CrossRef]
5. Jung, S.; Park, Y.; Lee, Y. A Novel Approach to Investigate the Superheating Grain Refinement Process of Aluminum-Bearing Magnesium Alloys Using Rapid Solidification Process. *Materials* **2023**, *16*, 4799. [CrossRef]
6. Shen, G.; Xiang, Z.; Ma, X.; Huang, J.; Zhao, Y.; Li, J.; Wang, Z.; Shi, G.; Chen, Z. Investigation of Microstructures and Mechanical Properties of Ultra-High Strength Al-Zn-Mg-Cu Alloy Prepared by Rapid Solidification and Hot Extrusion. *Metals* **2023**, *13*, 293. [CrossRef]
7. Chaieb, O.; Olufayo, O.A.; Songmene, V.; Jahazi, M. Investigation on Surface Quality of a Rapidly Solidified Al–50%Si Alloy Component for Deep-Space Applications. *Materials* **2022**, *13*, 3412. [CrossRef]
8. Okugawa, M.; Furushiro, Y.; Koizumi, Y. Effect of Rapid Heating and Cooling Conditions on Microstructure Formation in Powder Bed Fusion of Al-Si Hypoeutectic Alloy: A Phase-Field Study. *Materials* **2022**, *15*, 6092. [CrossRef] [PubMed]
9. Peng, Q.; Yang, B.; Milkereit, B.; Liu, D.; Spronger, A.; Rettenmayr, M.; Schick, C.; Keßler, O. Nucleation Behavior of a Single Al-20Si Particle Rapidly Solidified in a Fast Scanning Calorimeter. *Materials* **2021**, *14*, 2920. [CrossRef] [PubMed]

10. Gerland, S.; Raatz, A. Adhesive Bonding of an Aluminum Alloy with and without an Oxide Layer in Atmospheres with Different Oxygen Contents. *Appl. Sci.* **2022**, *13*, 547. [CrossRef]
11. Bolzoni, L.; Babu, N.H. Engineering the heterogeneous nuclei in Al-Si alloys for solidification control. *Appl. Mater. Today* **2016**, *5*, 255–259. [CrossRef]
12. Bolzoni, L.; Hari Babu, N. Efficacy of Borides in Grain Refining Al-Si Alloys. *Metall. Mater. Trans. A* **2019**, *50*, 746–756. [CrossRef]
13. Maxwell, I.; Hellawell, A. A Simple Model for Grain Refinement During Solidification. *Acta Metall.* **1975**, *23*, 229–237. [CrossRef]
14. Sunitha, K.; Gurusami, K. Study of Al-Si alloys grain refinement by inoculation. *Mater. Today* **2021**, *43*, 1825–1829. [CrossRef]
15. Zhao, C.; Li, Y.; Xu, J.; Luo, Q.; Jiang, Y.; Xiao, Q.; Li, Q. Enhanced grain refinement of Al-Si alloys by novel Al-V-B refiners. *J. Mater. Sci. Technol.* **2021**, *94*, 104–112. [CrossRef]
16. Lumley, R. *Fundamentals of Aluminium Metallurgy: Production, Processing, and Applications*; Woodhead Publishing Limited: Cambridge, UK, 2010.
17. Wang, Y.; Fang, C.M.; Zhou, L.; Hashimoto, T.; Zhou, X.; Ramasse, Q.M.; Fan, Z. Mechanism for Zr poisoning of Al-Ti-B based grain refiners. *Acta Mater.* **2019**, *164*, 428–439. [CrossRef]
18. Perepezko, J.E.; LeBeau, S.L. Nucleation of Al During Solidification. In Proceedings of the 2nd International Symposium "Al-Transformation Technology and Applications", Buenos Aires, Argentina, 24–24 August 1981; pp. 309–346.
19. Guzowski, M.M.; Sigworth, G.K.; Sentner, D.A. The role of boron in the grain refinement of aluminum with titanium. *Metall. Trans. A* **1987**, *18*, 603–619. [CrossRef]
20. Easton, M.; StJohn, D.H. Grain refinement of aluminum alloys: Part I. The nucleant and solute paradigms—A review of the literature. *Metall. Mater.Trans. A* **1999**, *30*, 1613–1623. [CrossRef]
21. Jones, G.P.; Pearson, J. Factors affecting grain refinement of aluminium using Ti and B Additives. *Metall. Mater. Trans. B* **1976**, *7*, 223–234. [CrossRef]
22. StJohn, D.H.; Hogan, L.M. Al3Ti and the grain refinement of aluminum. *J. Aust. Inst. Metals* **1977**, *22*, 160–166.
23. Easton, M.; StJohn, D. An analysis of the relationship between grain size, solute content, and the potency and number density of nucleant particles. *Metall. Trans. A* **2005**, *36*, 1911–1920. [CrossRef]
24. Greer, A.L.; Cooper, P.S.; Meredith, M.W.; Schneider, W.; Schumacher, P.; Spittle, J.A.; Tronche, A. Grain refinement of aluminium alloys by inoculation. *Adv. Eng. Mater.* **2003**, *5*, 81–91. [CrossRef]
25. Birch, M.E.J.; Fisher, P. *Aluminum Technology*; The Institute of Metals: London, UK, 1986; p. 117.
26. Greer, A.L.; Bunn, A.M.; Tronche, A.; Evans, P.V.; Bristow, D.J. Modelling of inoculation of metallic melts: Application to grain refinement of aluminium by Al–Ti–B. *Acta Mater.* **2000**, *48*, 2823–2835. [CrossRef]
27. Quested, T.E.; Greer, A.L. The effect of the size distribution of inoculant particles on as-cast grain size in aluminium alloys. *Acta Mater.* **2004**, *52*, 3859–3868. [CrossRef]
28. Murty, B.S.; Kori, S.A.; Chakraborty, M. Grain refinement of aluminium and its alloys by heterogeneous nucleation and alloying. *Int. Mater. Rev.* **2002**, *47*, 3–29. [CrossRef]
29. Wei, Y.S.; Wang, C.; You, J.; Qiu, D.; Gao, Y.; Xu, H.; Xu, J.; Wang, H.Y. Substantial grain refinement of Al-Mn-Si alloys mediated by collaborative effect of Al-5Ti-1B refiner and sub-rapid solidification. *J. Mater. Sci. Technol.* **2024**, *187*, 230–239. [CrossRef]
30. Iqbal, N.; van Dijk, N.H.; Hansen, T.; Katgerman, L.; Kearley, G.J. The role of solute titanium and TiB2 particles in the liquid—Solid phase transformation of aluminum alloys. *Mater. Sci. Eng. A* **2004**, *386*, 20–26. [CrossRef]
31. Samuel, E.; Tahiri, H.; Samuel, A.M.; Songmene, V.; Samuel, F.H. *A Review on Fundamentals of Grain Refining of Al-Si Cast Alloys. Recent Advancements in Aluminum Alloys*; IntechOpen: London, UK, 2024. [CrossRef]
32. Tahiri, H.; Samuel, A.M.; Doty, H.W.; Valtierra, S.; Samuel, F.H. Effect of Sr–Grain Refiner–Si Interactions on the Microstructure Characteristics of Al–Si Hypereutectic Alloys. *Int. J. Met.* **2018**, *12*, 307–320. [CrossRef]
33. Nafisi, S.; Ghomashchi, R. Grain refining of conventional and semi-solid A356 Al–Si alloy. *J. Mater. Process. Technol.* **2006**, *174*, 371–383. [CrossRef]
34. Dong, X.; Ji, S. Si poisoning and promotion on the microstructure and mechanical properties of Al–Si–Mg cast alloys. *J. Mater. Sci.* **2018**, *53*, 7778–7792. [CrossRef]
35. Easton, M.A.; StJohn, D.H. A model of grain refinement incorporating alloy constitution and potency of heterogeneous nucleant particles. *Acta Mater.* **2001**, *49*, 1867–1878. [CrossRef]
36. Qian, M.; Cao, P.; Easton, M.A.; McDonald, S.D.; StJohn, D.H. An analytical model for constitutional supercooling-driven grain formation and grain size prediction. *Acta Mater.* **2010**, *58*, 3262–3270. [CrossRef]
37. Men, H.; Fan, Z. Effects of solute content on grain refinement in an isothermal melt. *Acta Mater.* **2011**, *59*, 2704–2712. [CrossRef]
38. StJohn, D.H.; Qian, M.; Easton, M.A.; Cao, P. The Interdependence Theory: The relationship between grain formation and nucleant selection. *Acta Mater.* **2011**, *59*, 4907–4921. [CrossRef]
39. Mohanty, P.S.; Samuel, F.H.; Gruzleski, J.E. Experimental study on pore nucleation by inclusions in aluminum castings. *Am. Foundrymen's Soc.* **1995**, *99*, 555–564.
40. Zhang, Y.H.; Ye, C.Y.; Shen, Y.P.; Chang, W.; StJohn, D.H.; Wang, G.; Zhai, Q.J. Grain refinement of hypoeutectic Al-7wt.%Si alloy induced by an Al–V–B master alloy. *J. Alloys Compd.* **2020**, *812*, 152022. [CrossRef]
41. Nadendla, H.B.; Nowak, M.; Bolzoni, L. Grain Refiner for Al-Si Alloys. In *Light Metals 2013*; The Minerals, Metals & Materials Series; Sadler, B.A., Ed.; Springer: Cham, Switzerland, 2016. [CrossRef]

42. Li, Y.; Jiang, Y.; Hu, B.; Li, Q. Novel Al-Ti-Nb-B grain refiners with superior efficiency for Al-Si alloys. *Scr. Mater.* **2020**, *187*, 262–267. [CrossRef]
43. Nafisi, S.; Ghomashchi, R. Boron-based refiners: Implications in conventional casting of Al–Si alloys. *Mater. Sci. Eng. A* **2007**, *452*, 445–453. [CrossRef]
44. Nakao, Y.; Kobayashi, T.; Okumura, A. Effects of TiC, TaC, WC, TaC-WC, NbC and VC on Grain Refining of Pure Aluminum and Its Alloys. *J. Jpn. Inst. Light Met.* **1970**, *20*, 163–175. [CrossRef]
45. Davies, I.G.; Dennis, J.M.; Hellawell, A. The Nucleation of Aluminum Grains in Alloys of Aluminum with Titanium and Boron. *Metall. Trans.* **1970**, *1*, 275–280. [CrossRef]
46. Zhang, D.L.; Cantor, B. The Effect of Dopants on the Heterogeneous Nucleation of the Solidification of Cd and Pb Particles Embedded in an Al Matrix. *Acta Metall. Mater.* **1992**, *40*, 2951–2960. [CrossRef]
47. Glicksman, M.E.; Childs, W.J. Nucleation Catalysis in Supercooled Liquid Tin. *Acta Metall.* **1962**, *10*, 925–933. [CrossRef]
48. Porter, D.A.; Easterling, E. *Phase Transformations in Metals and Alloys*; Chapman & Hall: London, UK, 1992; pp. 192–197.
49. Tøndel, P.A.; Arnberg, L. Grain refinement of an Al-10%Si alloy by Ti-additions. In Proceedings of the The 3rd International Conference on Aluminium Alloys, Yokohama, Japan, 5–9 September 2010; pp. 129–134.
50. Birol, Y. The effect of holding conditions in the conventional halide salt process on the performance of Al–Ti–B grain refiner alloys. *J. Alloys Compd.* **2007**, *427*, 142–147. [CrossRef]
51. Yan, M.; Luo, W. Effects of grain refinement on the rheological behaviors of semisolid hypoeutectic Al–Si alloys. *Mater. Chem. Phys.* **2007**, *104*, 267–270. [CrossRef]
52. Gao, M.; Zhao, X.; Gao, A.; Li, R.; Chen, W.; Gao, M.; Liang, S.; Li, H. Effect of Si Content on the Morphology Evolution of the Si Primary Dendrites in Al-Si Alloy Solvent Refining Process. *Silicon* **2022**, *14*, 4501–4508. [CrossRef]
53. Peng, W.; Du, Q.; Wu, G.; Dan, W.; Hu, W.; Zhang, J. The role of Ti and Si in the nucleation of α-Al during hot dip coating of steel with Al–43.4wt.%Zn–1.6wt.%Si alloy. *Surf. Coat. Technol.* **2016**, *299*, 56–64. [CrossRef]
54. Mondolfo, L.F.; Barlock, J.G. Effect of superheating on structure of some aluminum alloys. *Metall. Trans. B Décembre* **1975**, *6B*, 565–572. [CrossRef]
55. Taylor, J.A.; Wang, H.; StJohn, D.H.; Bainbridge, I.F. Anomalous grain coarsening behaviour in grain-refined aluminium alloys cast using low superheat. In *Light Metals*; Angier, J., Ed.; TMS: Warrendale, PA, USA, 2001; pp. 935–941.
56. Bäckerud, L.; Chai, G.; Tamminen, J. *Solidification Characteristics of Aluminium Alloys, Vol. 2: Foundry Alloys*; AFS/Skanaluminium: Des Plaines, IL, USA, 1990; pp. 71–84.
57. Li, Q.; Liu, X.; Wang, J.; Xue, C.; Wang, S. Boosting the grain refinement of commercial Al alloys by compound addition of Sc. *J. Mater. Res. Technol.* **2024**, *28*, 1774–1783. [CrossRef]
58. Spittle, J.A.; Keeble, J.M.; Meshhedani, A.L. The grain refinement of Al-Si foundry alloys. *TMS Light Met.* **1997**, *1997*, 795–800.
59. Sigworth, G.K.; Guzowski, M.M. Grain refining of hypoeutectic Al-Si alloys. *AFS Trans.* **1985**, *93*, 907–912.
60. Schumacher, P.; McKay, B. *Solidification of Aluminum Alloys*; Chu, G., Douglas, A., Granger, H.Q., Eds.; TMS: Pittsburgh, PA, USA, 2004.
61. Wang, Y.; Que, Z.; Hashimoto, T.; Zhou, X.; Fan, Z. Mechanism for Si Poisoning of Al-Ti-B Grain Refiners in Al Alloys. *Metall. Mater. Trans. A* **2020**, *51*, 5743–5757. [CrossRef]
62. Kori, S.A.; Murty, B.S.; Chakraborty, M. Development of an efficient grain refiner for Al-7Si alloy and its modification with strontium. *Mater. Sci. Eng. A* **2000**, *283*, 94–104. [CrossRef]
63. Cooper, P.; Hardman, A.; Boot, D.; Burhop, E. Characterisation of a new generation of grain refiners for the foundry industry. In *Light Metals*; Crepeau, P.N., Ed.; TMS: San Diego, CA, USA, 2003; pp. 923–928.
64. Jin, S.; Luo, Z.; An, X.; Liao, X.; Li, J.; Sha, G. Composition-dependent dynamic precipitation and grain refinement in Al-Si system under high-pressure torsion. *J. Mater. Sci. Technol.* **2021**, *68*, 199–208. [CrossRef]
65. Massalski, T.B.; Okamoto, H.; Subramanian, P.R.; Kacprzak, L. (Eds.) *Binary Alloy Phase Diagrams*, 2nd ed.; ASM International: Almere, The Netherlands, 1990; p. 540.
66. Gwalani, B.; Fu, W.; Olszta, M.; Silverstein, J.; Yadav, D.R.; Manimunda, P.; Guzman, A.; Xie, K.; Rohatgi, A.; Mathaudhu, S.; et al. Lattice misorientation evolution and grain refinement in Al-Si alloys under high-strain shear deformation. *Materialia* **2021**, *18*, 101146. [CrossRef]
67. Qiu, D.; Taylor, J.A.; Zhang, M.X.; Kelly, P.M. A mechanism for the poisoning effect of silicon on the grain refinement of Al–Si alloys. *Acta Mater.* **2007**, *55*, 1447–1456. [CrossRef]
68. Liao, H.; Sun, Y.S.E.G. Effect of Al-5Ti-1B on the microstructure of near-eutectic Al-13%Si alloys modified with Sr. *J. Mater. Sci.* **2002**, *37*, 3489–3495. [CrossRef]
69. Sukow, C.A.; Nemanich, R.J. Morphology of $TiSi_2$ and $ZrSi_2$ on Si(100) and (111) surfaces. *Mater. Res. Soc.* **1994**, *9*, 1214–1227. [CrossRef]
70. Iida, T.; Koma, M.; Ohwa, Y.; Shudo, K.; Tanaka, S.O.E.M. Observation of thermal growth of silicide on titanium-deposited silicon surfaces. *Surf. Sci.* **2007**, *601*, 4444–4448. [CrossRef]
71. Njuguna, B.K.; Li, J.Y.; Tan, Y.; Sun, Q.Q.; Li, P.T. Grain refinement of primary silicon in hypereutectic Al-Si alloys by different P-containing compounds. *China Foundry* **2021**, *18*, 37–44. [CrossRef]
72. Knaislová, A.; Michna, Š.; Hren, I.; Vlach, T.; Michalcová, A.; Novák, P.; Stančeková, D. Microstructural Characteristics of Al-Ti-B Inoculation Wires and Their Addition to the $AlSi_7Mg_{0.3}$ Alloy. *Materials* **2022**, *15*, 7626. [CrossRef]

73. Sumalatha, C.; Rao, P.; Rao, V.; Deepak, M. Influence of Grain Refiner, Modifier and Graphene on the Dry Sliding Wear of Hypereutectic Al–Si Alloys. *Metallogr. Microstruct. Anal.* **2022**, *11*, 234–244. [CrossRef]
74. Sumalatha, C.; Rao, P.C.S.; Rao, V.; Deepak, M.S.K. Effect of grain refiner, modifier and graphene on the mechanical properties of hyper eutectic Al-Si alloys by experimental and numerical investigation. *Mater. Today Proc.* **2022**, *62*, 3891. [CrossRef]
75. Johnsson, M. Grain refinement of aluminium studied by use of a thermal analytical technique. *Thermochimica acta* **1995**, *256*, 107–121. [CrossRef]
76. Johnsson, M.; Backerud, L.; Sigworth, G.K. Study of the mechanism of grain refinement of aluminum after additions of Ti- and B-containing master alloys. *Metall. Trans. A* **1993**, *24*, 481–491. [CrossRef]
77. Bian, H.; Aoyagi, K.; Zhao, Y.; Maeda, C.; Mouri, T.; Chiba, A. Microstructure refinement for superior ductility of Al–Si alloy by electron beam melting. *Addit. Manuf.* **2020**, *32*, 100982. [CrossRef]
78. Li, Y.; Jiang, Y.; Liu, B.; Luo, Q.; Hu, B.; Li, Q. Understanding grain refining and anti Si-poisoning effect in Al-10Si/Al-5Nb-B system. *J. Mater. Sci. Technol.* **2021**, *65*, 190–201. [CrossRef]

Disclaimer/Publisher's Note: The statements, opinions and data contained in all publications are solely those of the individual author(s) and contributor(s) and not of MDPI and/or the editor(s). MDPI and/or the editor(s) disclaim responsibility for any injury to people or property resulting from any ideas, methods, instructions or products referred to in the content.